Characterization of axially-symmetric magnetic fields

Candidate:

Mario KAZAZI

CERN Supervisor:

Dr. Marco Buzio

University Supervisor:

Ch.mo prof. Pasquale ARPAIA

This thesis is dedicated to my parents.
For their endless love, support and encouragement

Resume

In solenoids for particle accelerators, the magnetic field is usually mapped by means of 3D Hall-sensing systems through a burdensome and costly procedure. A further problem arises from a coherent treatment between the beam physics requirements, the qualification of numerical models, the design and manufacturing of the magnet, and the magnetic measurements. For example, when the magnet is misaligned with respect to the longitudinal direction of the mapper, the fringe field shows spurious components.

A method was therefore developed for measuring the magnetic field of axially-symmetric magnets by exploiting their inherent symmetry. The method yields a measurement of the magnetic flux linked with a pair of sensing coils as a function of their longitudinal position.

An induction transducer, sensitive to the longitudinal and radial components of the solenoid under test, has been designed and constructed. A transport system moves the transducer along the magnet axis, covering the full length of the magnet and including the fringe field. The induced voltage is acquired and integrated digitally in order to yield the flux linkage as a function of the linear position, measured by a laser interferometer. The re-parametrization related to intrinsic relationship between the motion time and the linear translation position along the magnet axis relaxes the requirements on the homogeneous motion of the transport system.

After a proof-of-principle demonstration, the uncertainty sources affecting the measurement system were evaluated and their influence on the result assessed. In particular, the measurement model for the translating-coils method is formulated and a Sequential Monte–Carlo algorithm, based on Bayesian inference, is then used to dynamically estimate the distribution of the output quantity, starting from the knowledge of the distributions of all the uncertainty sources considered in the model.

According to the indications of the uncertainty analysis results, a translating-coils system was prototyped and integrated in the existing CERN platform, which includes

Fast Digital Integrators (FDIs), an encoder board, a motor controller, and the Flexible Framework for Magnetic Measurement (FFMM).

The system was validated in a reference solenoid by pointing out more than satisfying agreement of the results. Finally, the system has been employed in challenging measurements on the field, resulting in a reliable and accurate method for the characterization of axially-symmetric magnet systems.

Keywords: magnetic measurements, axially-symmetric magnets, induction transducer, translating coils, uncertainty analysis, particle filter, experimental validation.

List of publications

List of the publications of the candidate:

- P. Arpaia, M. Buzio, M. Kazazi, S. Russenschuck, "A fluxmeter based on translating coils for axially-symmetric magnets", *20th IMEKO TC4*, Benevento, Italy, Sept 15-17, 2014;
- P. Arpaia, M. Buzio, L. De Vito, M. Kazazi, and S. Russenschuck. "Uncertainty analysis for a moving Fluxmeter", *XXI IMEKO World Congress*, August 30 - September 4, 2015, Prague, Czech Republic;
- P. Arpaia, M. Buzio, M. Kazazi, S. Russenschuck, "Proof-of-principle demonstration of a translating coils-based method for measuring the magnetic field of axially-symmetric magnets", Journal of Instrumentation, 10(02), 2015.
- P. Arpaia, L. De Vito, and M. Kazazi. "Dynamic measurement and uncertainty analysis of the magnetic field for axially-symmetric magnets by means of a particle filter", Metrologia, [submitted], 2016.
- P. Arpaia, M. Buzio, M. Kazazi, S. Russenschuck, "Measurement system based on translating coils for testing axially-symmetric magnets", Journal of Instrumentation, [submitted], 2016.

Acknowledgments

The work presented in this thesis was carried out in the framework of a collaboration between the Engineering Department of the University of Sannio (Benevento, Italy) and the Magnetic Measurement section of the Magnets, Superconductors and Cryostats group (TE-MSC-MM) at CERN. This experience represented for me a great opportunity of growth, both from the professional and the human point of view. I worked with bright engineers from whom I have learned a lot, and the whole team is gratefully acknowledged.

I would first like to thank my supervisor Prof. Pasquale Arpaia for affording me the opportunity to work with him at CERN and for his guidance throughout my PhD research studies. I am grateful for his support and encouragement during difficult times, and for transmitting to me his passion for research.
I want to thank my CERN Supervisor Marco Buzio for his brilliant and constructive suggestions, which were determinant for the accomplishment of the work presented in this thesis.
A special thanks goes to the section leader Stephan Russenschuck. He has given me superb scientific guidance, many insightful suggestions and demonstrated a sincere interest in my work.

I thank the group leader Luca Bottura, who took time out of his busy schedule to meet me and provide insightful discussions about my research.
I am also very grateful to my PhD University Coordinator Prof. Luigi Glielmo for his precious help to organize a special PhD commission in order to allow me to meet the deadline for a post-doc position at the CEA.

This thesis owes much to the close and fruitful collaboration with the TE-MSC-MM section people at CERN. I gratefully acknowledge to the entire TE-MSC-MM section at CERN for their support and for their kind availability to help me in my technical problems (Olaf, David, Peter, Riccardo, Manu, Naim, Xavier).

I want to thank Prof. Luca De Vito, who patiently guided my study of uncertainty analysis.

I will forever be thankful to Lucio Fiscarelli for the many discussions that helped me understand my research area better, and for listening to me no matter how busy or tired he was. Most of the results described in this thesis were accomplished with his help and support.

Many thanks to Carlo Petrone, Giancarlo Golluccio and Giuseppe Montenero, for their help and support. They provided a friendly and cooperative atmosphere at work and also useful feedback and insightful comments on my work.
To my friends and colleagues at CERN, thanks for the fun and support! To Domenico Caiazza, Mario Girone, Ernesto De Matteis and Giordana Severino, I will easily miss hanging out with you and the funny moments in the office. I wish to sincerely thank Oliver Köster for being a best friend and for the great time in the office and outside. I am also very grateful to the "Equipo" teammates, Vincenzo Daponte, Carlo Baccigalupi, Andrea Passarelli, Nicola Cardines, Antonio Pacheco, for the great moments and their friendship. A special thanks to all the colleagues/friends, Emmanuele Ravaioli, Alessandro Parrella, Daniele for the mechanical design of the bench, Martino, Marco, and Rocio.

I would like to dedicate this thesis to my family. I have been extremely fortunate in my life to have a family who has shown me unconditional love and support.
Prindërit e mi të mrekullueshëm Mimoza dhe Ermiri dhe vëllai im Xhino meritojnë një falenderim të veçantë për mbështetjen dhe përkrahjen në çdo hap të jetës sime.

Dulcis in fundo, a very special acknowledgement goes to my girlfriend Viktoria for her love and patience while I was working on this dissertation. Viki, no words in this thesis or elsewhere can express what you mean to me.

Mario Kazazi

Contents

Introduction

In magnetic systems for particle accelerators, the measurement of the magnetic field is often the final verification of a complex design and fabrication process [1]. Besides the magnet prototyping phase, field measurements are important at different stages of an accelerator project. The stability of the particle beam is affected critically by magnetic field errors, and therefore very-accurate measurements are necessary to guarantee that the required field strength, shape and homogeneity have been achieved in the bending and focusing magnets. Moreover, although magnetic systems are optimized thanks to powerful computational tools at their design stage, direct measurements of the magnetic field are the only way to guarantee that the target field quality is reached.

Other than in the low-energy section of particle accelerators [2], an axially-symmetric (axisymmetric) magnet is often used to focus charged particle beams in other devices, such as electron microscopes [3], electron guns [4], or image intensifiers. Other potential applications are related to laser-accelerated protons or ions [5] [6] - for example, in particle therapy or short-pulse radiographic diagnostics - where axisymmetric magnets are used for effective focusing and energy selection.

By using solenoids in transport channels quite modest emittance growth can be achieved. Controlling the emittance growth is required to reduce particle losses in high-power accelerators, where axially-symmetric focusing elements with short periods have to be used. In fact, this solution often works better than sequential pairs of quadrupoles that give rise to significant halo formation [7]. Particles moving exactly along the magnetic axis do not experience a Lorentz force. Off-axis particles are azimuthally accelerated by the radial field component in the end regions of the magnet. The resulting helical motion in the longitudinal field of the magnet center yields a focusing effect due to the radial Lorentz force.

Employing axisymmetric lenses to provide the required focusing strength for charged particle beams imposes strict requirements on magnetic field measurement and axis determination. Therefore, a characterization of the magnetic field is clearly paramount for lattice design calculations.

Axisymmetric magnets are hardly compatible with standard instrumentation optimized for accelerator multipole magnets and are routinely tested with general-purpose instruments, such as 3D Hall-probe mapping systems [8] [9]. However, these systems are poorly adapted to exploit their inherent symmetry. Analogously, available state-of-the-art stretched [10] [11] and vibrating-wire [12] systems, only provide information about integral field properties.

The work for this PhD dissertation deals with an original translating-coils method for measuring axisymmetric magnetic fields. Correspondingly, an automatic measurement system based on the translating-coils method was designed, prototyped, experimentally validated and exploited on the field for testing axi-symmetric magnets. The system yields an accurate measurement of the integrals of the longitudinal and transverse field components as a function of the longitudinal position in a fraction of the time needed by traditional techniques. The development of such a system has involved the successful completion of the following tasks:

- **Development of the translating-coils measurement method** [13]. An induction transducer, sensitive to the longitudinal and radial components of solenoids, translates along the magnet axis and the induced voltage is integrated between predefined positions.

- **Proof-of-principle demonstration** [14]. The results obtained with a preliminary measurement setup are used to validate the measurement concept of the method.

- **Uncertainty analysis** [15] [16]. The main uncertainty sources are analyzed and a particle filter is used to estimate their propagation in the distribution of the output quantity.

- **Realization of the measurement bench** [17]. The prototype of the measurement system is automatized and integrated with the CERN platform for magnetic measurements. Hardware components and C++ code controlling different sensors and equipment are developed.

- **Experimental validation**. The measurements results of the translating-coils system are validated in comparison to a reference solenoid magnet.

- **On-field exploitation**. The measurement system is employed in challenging applications, showing satisfying results where other measurement methods resulted not adapted.

The Thesis is organized as it follows.
The *Background* part deals with a general introduction to axisymmetric magnets. In particular, **Chapter 1** presents the characteristics and the main applications of these magnets in particle accelerator facilities. **Chapter 2** reviews the principal measurement methods used today for measuring axially-symmetric magnetic fields.

In the *Proposal* part, **Chapter 3** describes the working principle of the translating-coils method and the main components of system. The induction transducer, the transport system and the position measurement system are also illustrated. **Chapter 4** deals with the proof-of-principle demonstration of the method and a preliminary experimental validation. After the successful proof-of-principle demonstration, in **Chapter 5** the main uncertainty sources are analyzed and a model of the measurement process is defined. A Sequential Monte-Carlo method based on Bayesian inference is then used to dynamically estimate the distribution of the output quantity, starting from the knowledge of the distributions of all the uncertainty sources considered in the model.

The *Experimental Results* part presents the measurement system and the results obtained. The final prototype of the system and its architecture are described in **Chapter 6**, where mechanics and electronics components were improved, according to the suggestions of the uncertainty analysis results. In **Chapter 7**, the measurements results and experimental validation of the system are discussed, by checking the results against a reference solenoid. Finally, **Chapter 8** reports on-field applications of the translating-coils measurement system, by highlighting its effectiveness in the characterization of axially-symmetric magnets.

Part I

Background

Chapter 1

Axially-symmetric magnetic systems

In the particle accelerator research community, the interest in understanding the focusing and transfer characteristics of resistive and superconducting axisymmetric magnets is growing more and more. Magnetic elements such as solenoids are used in the accelerators at various places for focusing and transporting charged particle beams. In the following, the focusing characteristics and the main applications of these magnets are described.

1.1 Focusing

An axially-symmetric magnetic lens consists of a region of cylindrically-symmetric, radial, and axial magnetic fields produced by axi-centered coils (Fig. 1.1). The

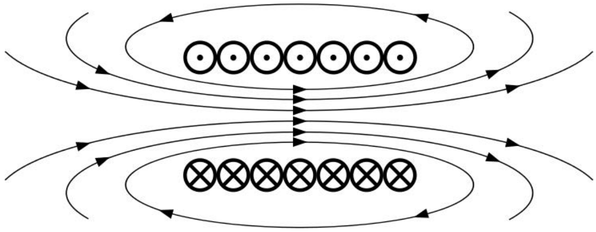

Figure 1.1: Schematic of the field lines of a solenoid

dominant component in the solenoid field is the axial component, which has maximum strength at the center of the solenoid and reduces towards the ends. The axial field, being parallel to the longitudinal velocity of the charged particles, could not give rise to the Lorentz force by interacting with the axial velocity component. However, at the entrance and at the exit of a solenoid, a radial field component generating an azimuthal velocity component exists. This velocity component, in turn, interacts with the axial field inside the solenoid and gives rise to a radial Lorentz force. As shown in Fig. 1.2, this force, which can be shown to be linearly dependent on the radial distance for paraxial rays, focuses the particles radially [18]. This approach provides simultaneous focusing in both the transverse planes and at the same time produce a rotation of the beam around the axis. For a cylindrically-symmetric magnet, the focusing process is described according to a thin-lens approximation by the following expressions of the rotation φ_L of the beam about the z-axis (the so-called Larmor angle):

$$\varphi_L = \frac{e}{2\gamma m v_z} \int_{z_1}^{z_2} B_z \mathrm{d}z = \frac{e}{2\gamma m v_z} F_1, \tag{1.1}$$

and the focusing strength $1/f$ [19]:

$$\frac{1}{f} = \frac{e^2}{4\gamma^2 m^2 v_z^2} \int_{z_1}^{z_2} B_z^2 \mathrm{d}z = \frac{e^2}{4\gamma^2 m^2 v_z^2} F_2 \tag{1.2}$$

where m is the electron rest mass, e the elementary charge, $\gamma = (1-\beta^2)^{-1/2}$, $\beta = v/c$ with v as particle velocity, c the speed of light in vacuum, and F_1 and F_2 the field integrals.

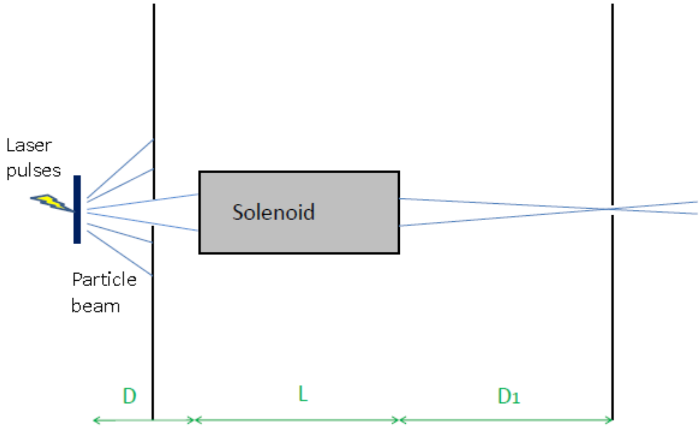

Figure 1.2: Focusing solenoid after a laser source.

1.2 Axially-symmetric magnetic lens for particle accelerators

Axially-symmetric magnetic lenses are applied at an increasing rate in low-energy beam transport (LEBT) sections of high-energy accelerators and in modern radio-frequency (RF) linear accelerators (linacs), for the purpose of emittance compensation, transverse focusing and electron cooling.

Many of these applications demand uniformity of magnetic field generated by solenoids within a volume of interest [20]. This is the case for Nuclear Magnetic Resonance (NMR) and Magnetic Resonance Imaging (MRI). In order to obtain high-quality images, the high homogeneity of static magnetic field in the desired imaging volume is required. In this case, the desired uniformity of magnetic field inside a solenoid is realized by means of structural modifications along with the magnetic flux concentrator rings at the coil ends [21].

Other applications, subject of study in this dissertation, demand a precise strength and shape of the magnetic field, characteristics that determine the beam focusing properties of the magnet. The solenoid specifications like field integrals, center fields and bore diameters depend on the beam characteristics and hence span wide ranges. These requirements determine which type and technology of axisymmetric magnet is most appropriate for a given case. Fig. 1.3 illustrates a schematic overview of the state-of-the-art winding types and technologies employed in axially-symmetric magnets applications. An example of the employment of resistive solenoids as focusing

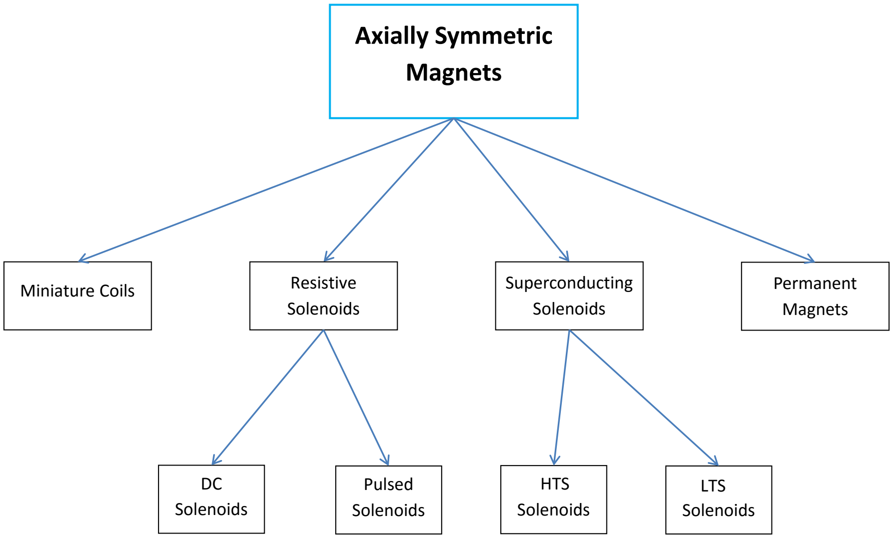

Figure 1.3: Type and technology classification of axially-symmetric magnets.

lenses in RF linacs are the Linac4 [22] and Linac3 [23] at CERN.

Linac4 is a 160 MeV normal-conducting linac for negative Hydrogen ions and the LEBT section is vital to control the current and emittance. In particular, the two solenoids highlighted in red in Fig. 1.4 are used to focus and to match the beam to the RFQ.

Linear accelerator 3 (Linac3) is the starting point in the heavy ion injector chain of the Large Hadron Collider (LHC), providing charged heavy ion beams for the CERN experimental program. Immediately after the ion source, a focusing solenoid (ITL.SOL01) is in charge of bringing a beam as small as possible to the spectrometer and avoid any loss of intensity [23].

Since the use of a solenoid as a focusing element is based on second order effects, it is desirable to go to higher magnetic field by employing superconducting (SC) devices to minimize the overall length occupied along the beamline [24].

In fact, for applications in SC RF accelerating structures, SC solenoid magnets are often preferred for their compact design and low remanent fringe fields. A compact accelerating-focusing lattice ca be obtained by using SC solenoids together with SC RF resonators within a common cryostat.

This solution has been adopted for the low energy part of a linac for the High

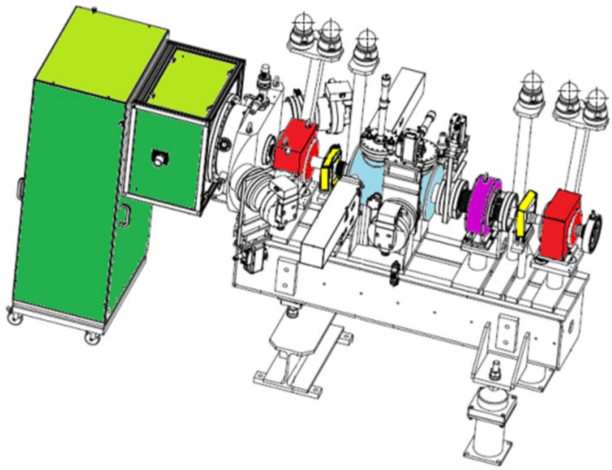

Figure 1.4: Sketch of the Linac4 LEBT [22].

Intensity Neutrino Source (HINS) project at Fermilab [25] [26], where SC focusing solenoids are installed inside RF cryomodules. Axially-symmetric focusing resulted in saving some longitudinal space, which is highly desired for beam line diagnostic equipment [27].

Two different superconducting solenoids, based respectively on High Temperature Superconductor (HTS) and Low Temperature Superconductor (LTS) coil technology, are presented in [28]. For the superconducting RF electron gun for the WiFEL at the University of Wisconsin [29] a low-field, large-bore 2G HTS solenoid for emittance compensation has been designed. As showed in Fig. 1.6, the unit is hence very compact and the solenoid operates safely at temperatures up to 70 K. For the High Intensity and Energy (HIE) upgrade of the ISOLDE facility at CERN [30], high-field LTS solenoids integrated in individual helium vessels have been designed and produced for the high-beta cryomodules.

Other examples of typical superconducting linacs, where solenoids are used for their simple design, easy production and low cost of manufacture, are ISAC-II in Canada [31] Project X of Fermilab [32] and Facility for Rare Isotope Beams (FRIB) of MSU in USA [33].

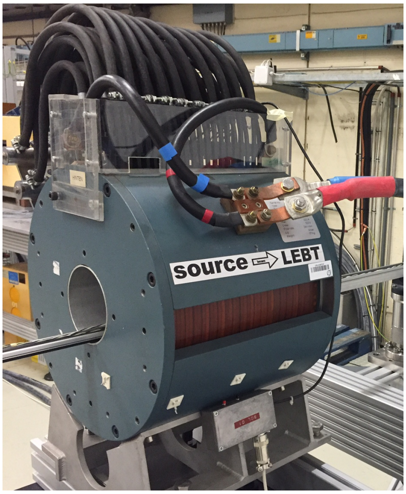

Figure 1.5: The ITL.SOL01 Linac3 solenoid.

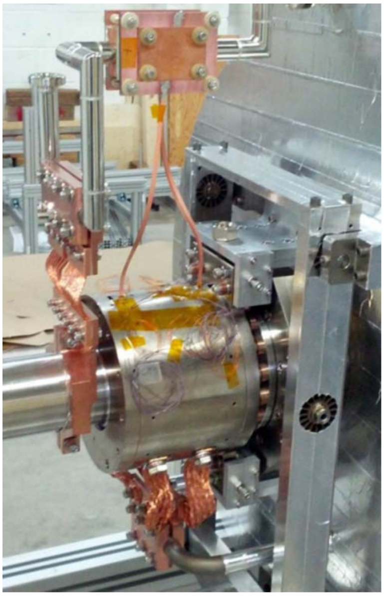

Figure 1.6: HTS solenoid mounted in position next to the SRF cavity in the electron gun at WiFEL, University of Wisconsin [28].

Chapter 2

Measurement methods for axially-symmetric magnets

Field errors in axisymmetric magnets have great influence on particle beam stability and quality. It has been demonstrated that residual emittance and longitudinal beam temperature are very sensitive to the magnetic field in almost all the applications presented in Chapter 1.

Employing axisymmetric lenses to provide the required focusing strength for charged particle beams imposes strict requirements on magnetic field measurement and axis determination. Therefore, reliable and efficient methods for measuring the magnetic field of focusing magnets are desired.

This chapter presents the principal methods available in literature for axisymmetric magnetic field measurement and axis determination, as classified in the tree diagram shown in Fig.2.1.

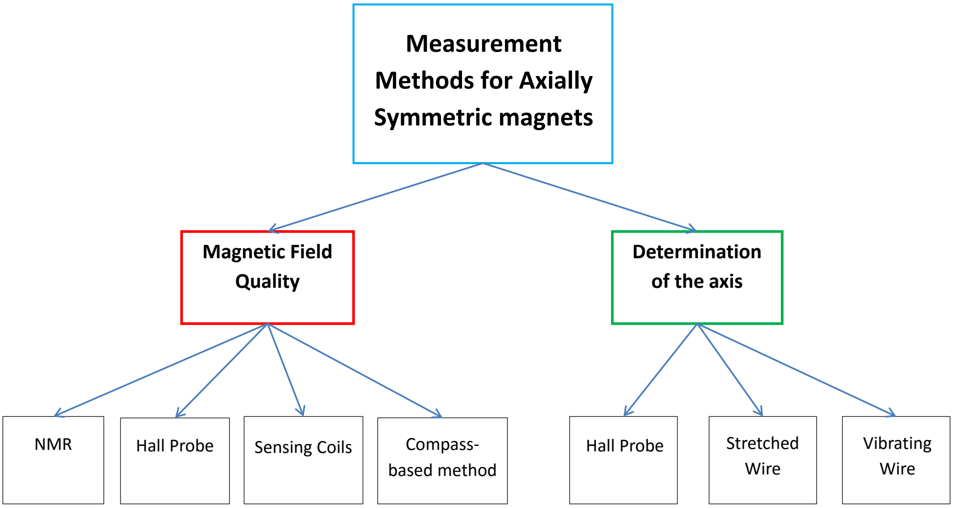

Figure 2.1: Commonly used measurements methods for axisymmetric magnetic fields.

2.1 Magnetic field quality

To measure the field quality of an axisymmetric magnet a precise characterization of the longitudinal and transversal field components is needed.

2.1.1 Hall-probe mapping systems

A combination of three Hall magnetic generators oriented in the three main directions and supported by three orthogonal plates (commonly defined as 3D Hall-probe) was and remains a way to measure simultaneously the three components of the magnetic field [34]. In the classical configuration, the Hall probe is attached to a measuring arm that can move with five degrees of freedom (three directions of translation and rotation around two axes). Usually the measurements are performed in a flying mode at a speed range of 10-50 mm/s. The voltages are recorded using a digital multimeters interfaced to a computer via a GPIB gateway. Finally, the data are post-processed off line using a defined calibration procedure described.

The Muon Ionization Cooling Experiment (MICE) is an R&D project that aims to demonstrate the cooling of muon beams. The MICE cooling channel is equipped with two spectrometer solenoids consisting of five superconducting Nb-Ti coils wound on a common aluminum mandrel. In [35], measurements of the axial and transverse components of the magnetic field through the warm bore of the magnet have been performed along the central magnet axis, and with horizontal and vertical offsets. A stainless steel guide tube has been used as a support for a 3D Hall-probe (Fig. 2.2) within the warm bore, as shown in Fig. 2.3. Another example of Hall-

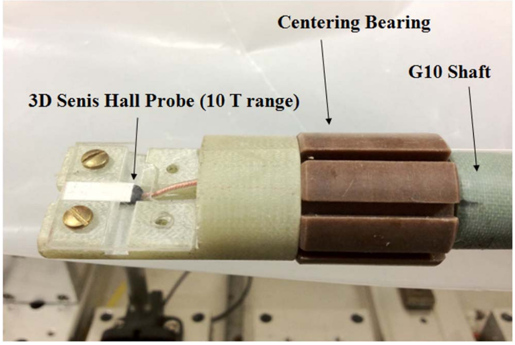

Figure 2.2: 3D Hall probe attached to G10 shaft with centering bearing [35].

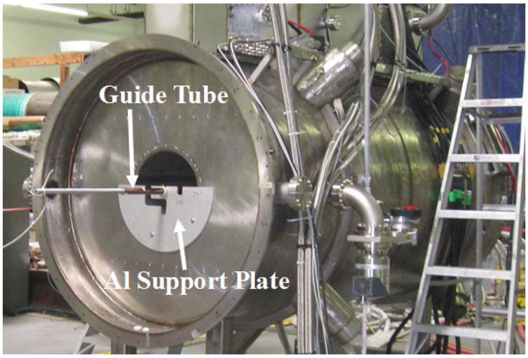

Figure 2.3: Measurement system [35].

probe measurement system explicitly designed for solenoids is described in [36]. The three-dimensional Hall-probe mapping system has been developed for measuring the solenoid magnet of the Pohang Light Source (PLS) photo-cathode RF e-gun. It can map the solenoid field either in Cartesian or in cylindrical coordinates system with a measurement reproducibility better than 0.5 G. The system has three axis motors: one for the azimuthal direction and the other two for the x and the z direction.

The first two accelerating sections of the SPARC Linac at the Frascati National Laboratories of INFN [37] are embedded in an array of 13 solenoids, required to produce a magnetic field for additional focusing in order to comply with the Ferrario working point matching conditions for emittance compensation.

As reported in [38], the magnetic field intensity of the focusing solenoids is measured by a Hall-probe system mounted on a 3D movement machine. Four out of five movement axes are motorized. By scanning the volume inside the solenoid it is possible to map the magnetic field in the zone of interest.

The Mu2e experiment at Fermilab is designed to explore charged lepton flavor violation by searching for muon-to-electron conversion. The magnetic field generated by a system of solenoids is a crucial component of Mu2e and requires accurate characterization to detect any potential flaws and to produce a detailed field map [39]. Fig. 2.4 illustrates the design for the Mu2e field mapping system. A precisely arranged set of Hall and NMR probes is mounted on a carriage to survey the magnetic field both azimuthally and axially. The carriage moves along precisely surveyed rails installed along the magnet axis, and stop at predefined positions. At each location the propeller arms rotates and stops at predefined angles to measure the magnetic field. To minimize positioning inaccuracies, linear and angular encoders coupled to a feedback control system can compensate for gear backlash and wear [40].

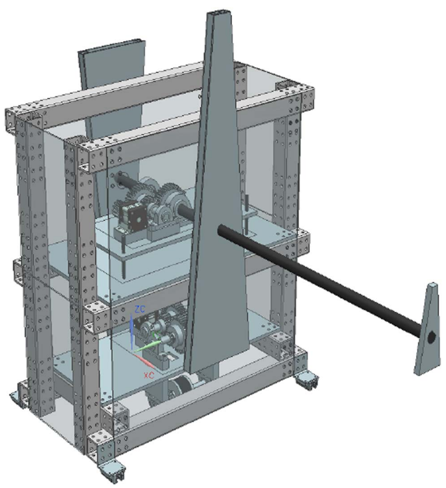

Figure 2.4: Mu2e field mapper design. Probes will be installed on two propeller arms. Propellers rotate to provide azimuthal coverage. The field mapper moves along the magnet axis to provide axial coverage [40].

2.1.2 Compass-based method

The prototype of the compass-based measuring system was designed and constructed at Budker Institute of Nuclear Physics (BINP) at Novosibirsk and then shipped to

Fermilab according to a mutual collaboration [41].

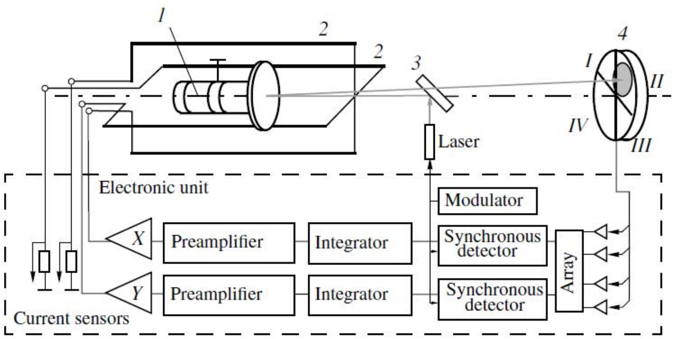

Figure 2.5: Diagram of the measuring device: (1) magnetic sensor, (2) conductors of the compensating circuits, (3) beam splitter, (4) photodetector, (I-IV) quadrants, and (X,Y) output current amplifiers [42].

Since that time it has being modified and improved, but the basic ideas are the same. A diagram of the measuring system is shown in Fig.2.6. The measuring circuit is an automatic control loop that incorporates an optomechanical magnetic sensor and a compensating system. A shift of the laser beam from the sensor's center induces an error signal that affects the currents in the conductors, compensating for the transverse field that is responsible for this shift. The transverse magnetic field components representing the local curvature of the field line are determined using the current amplitudes.

A detailed description of the measuring system has been presented by Bocharov et al. in [42].

The compass-based method has been used for the magnetic field measurement of the solenoid and its compensation in the Recycler Electron Cooler (REC) at Fermilab [43, 44]. The efficiency of the cooling process is governed by the quality of the guiding magnetic field produced by the solenoid in the cooling section and, therefore, a precise characterization of the transversal field is needed. The field components of the solenoid are measured by a specially designed compass-based sensor which is placed inside a cart that moves through the solenoid with a precision of 1 mm, providing a detailed field map [45].

Electron cooling is in use in many accelerators throughout the world. Several electron-cooling plants (electron coolers) have been designed and built in the last few years by the Budker Institute of Nuclear Physics for a number of foreign laboratories. The same measurement concept (magnetic needle-and-mirror) has been used to

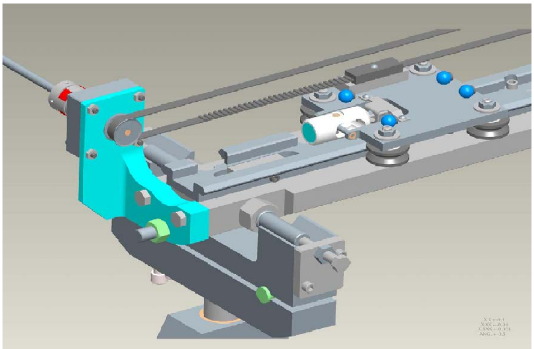

Figure 2.6: Carriage for Needle-and-Mirror.

measure the field straightness in the solenoids for the electron lens system for the Relativistic Heavy Ion Collider (RHIC) at Brookhaven National Laboratory (BNL). In this case the electron and proton beams must remain aligned to each other within < 50 microns as they pass through the solenoid. This places stringent requirement on the straightness of field lines in the solenoid and precise measurements of the field straightness are required to characterize the magnets, and to make the corrections [46, 47].

2.1.3 NMR

Methods based on NMR principles (imaging and spectroscopy) need a source of stationary magnetic field with minimal inhomogeneities. No magnet generates an ideal homogeneous magnetic field and therefore a complicated coil system construction fed by separate currents power supplies for compensation (shimming) of particular magnetic inhomogeneous components is needed.

In [48] is described a fast method for computation of feeding currents of shim coils for stationary magnetic field used in NMR imaging. The method needs to perform a magnetic field measurement in selected points of an assigned volume by using NMR magnetometers. The measurements were performed in three transversal planes on circles and their centers thanks to a probe positioning mask as showed in Fig. 2.7.

The development of a superconducting solenoid for a new Muonium HyperFine Structure (MuHFS) measurement at J-PARC requires an homogeneity of the magnetic field below 1 ppm within a spheroid region of 20 cm in diameter and 30 cm in length. In order to evaluate the field uniformity, a precise field monitoring system is presented in [49]. An NMR probe is used to measure the magnetic field and a 3-axis moving

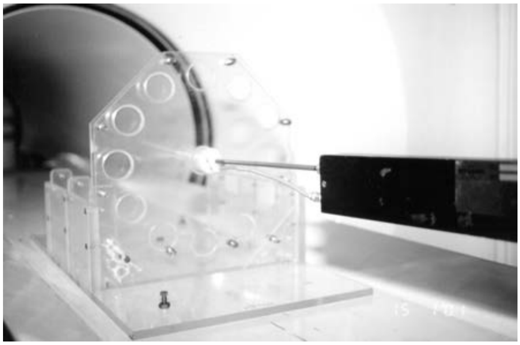

Figure 2.7: Measuring mask with holes for NMR magnetometer probe.

stage is designed for the probe positioning. Figure 2.8 shows the schematic view of the $r - \theta - z$ moving stage. The NMR probe is mounted on the slide stage in

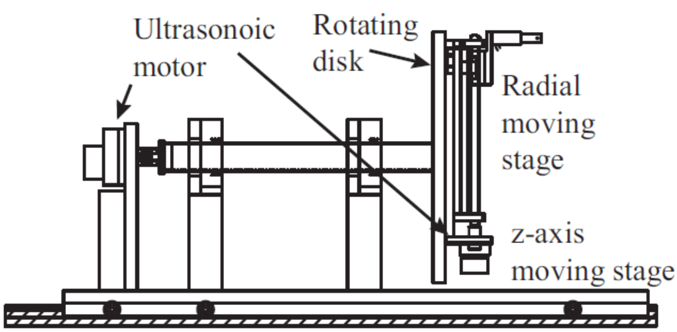

Figure 2.8: Schematic view of the moving stage [49].

radial direction, and the slide stage is mounted on a rotating disk. Both the radial slide stage and the rotating disk are driven by ultrasonic motors. The whole stage can move along the z- axis on the rail, and is driven by a stepping motor, which is 2 m away from the magnet end, far away enough so that there will be no significant distortion of the magnetic field. Almost all the parts of this system consist of non-metallic material except for the case of the ultrasonic motor and NMR probe, which are made by aluminum and copper.

2.2 Determination of the magnetic axis

For a proper and correct accelerator functioning it is important to align the focusing solenoids on the machine with their magnetic axes precisely coincident with the beam axis. Preliminary operations are therefore the geometrical characterization, to determine the geometrical axis, and the magnetic measurements, to determine the magnetic axis position with respect to the geometrical one.

2.2.1 Axis determination by Hall-probe systems

A common way to determine the magnetic axis is described in [50], where a Hall probe is rotated at several points along the axis of the solenoid, recording the measured field as a function of the rotation angle at each axial stop. Information about the displacement of the axis of rotation from the magnetic axis is obtained by analyzing the measured data.

The layout of the measurement setup is shown in Fig. 2.9. The drive shaft was connected to the probe assembly by a universal joint at one end, and to a PC controlled motor drive assembly at the other. This provided longitudinal and rotational motion of the probe.

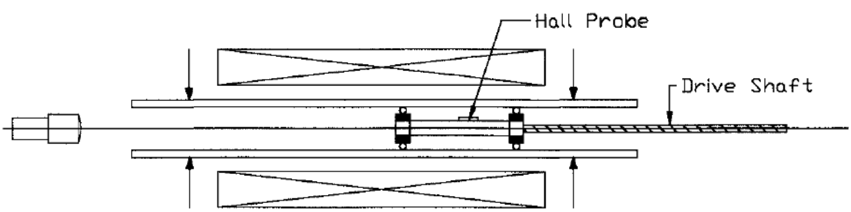

Figure 2.9: A layout of the measurement setup [50].

Another interesting method for axis determination by means of a Hall-probe system is presented in [51]. The magnetic center is calculated using the measured axial component of magnetic field B_z in Cartesian coordinate system because the accuracy of magnetic axis measurement could be improved significantly by using B_z, instead of the radial component of magnetic field B_r. To obtain the magnetic center, the measured two-dimensional field profiles at different positions along the z-axis were processed. Because the magnetic field was mapped in the x-y plane at a step of 1 mm, the measured data were interpolated. Then, the magnetic axes along the z-axis were calculated with a resolution of 0.01 mm using the conditions $\partial B_z/\partial x = \partial B_z/\partial y = 0$.

2.2.2 Single stretched-wire measurement method

The stretched-wire method, which is also relatively common, makes use of a single conducting wire stretched through the magnet and moved by precision translation stages at both ends, which are short circuited by a fixed wire. An integrator measures the induced loop voltage and the axis is obtained by iterating horizontal and vertical sweeps until symmetric start and end points are found, giving zero integrated flux.

The development of a high-current proton linac at FNAL went through many stages, starting from a pulsed 8 GeV linac, then to the HINS linac front end R&D, and now toward the ProjectX CW linac.

For different parts of the accelerator front end in each of these linacs, the design requires solenoid-based focusing lenses that can provide the needed transverse focusing on a very tight real estate environment. The multiple, often contradictory, design requirements of focusing lenses include the need for systematic measurements of the solenoid magnetic axis position.

J. DiMarco et al. reported in [52] [53] [54] alignment measurements made using Single Stretched Wire (SSW) techniques, which allow wire positioning control at the level of 1 micron.

2.2.3 Vibrating-wire measurement method

The vibrating-wire method is an evolution of the stretched wire method, in which transversal vibrations are continuously excited at the resonance frequencies of the wire, providing exceptional sensitivity. The vibrations are driven by an alternating current in a magnetic field.

In [55] [56], a method based on the vibrating-wire is proposed to center and align solenoid magnets.
The wire, fed by an alternating current, oscillates in a plane that is perpendicular to the transversal magnetic field. When the wire position coincides with the magnetic axis, the transversal field components cancel out and therefore no motion is induced. To center and align the solenoid two wire resonance frequencies are excited for co- and counter-directional movements of the wire stages. The procedure to find the minimum oscillation amplitudes is sensitive to misalignment in the micrometer range. The method is validated experimentally on a solenoid prototype for the Linac4 project at CERN (Fig. 2.10).

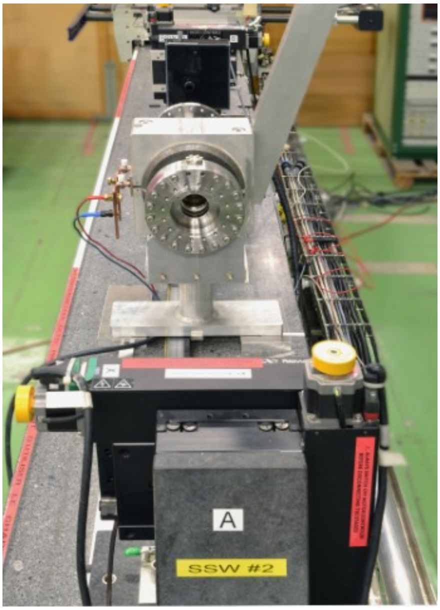

Figure 2.10: Vibrating wire measurement bench with mounted solenoid magnet under test [55].

Part II

Proposal

Chapter 3

Translating-coils measurement method

In this chapter, a measurement method based on translating sensing coils is proposed for mapping local field geometrical parameters with high accuracy. This measurement technique has not been used previously for axially symmetric magnets. The field integrals F_1 and F_2 are obtained more precisely and rapidly than by traditional techniques. In particular, the working principle and the architecture of the translating coil method are presented, by highlighting also the design of the induction transducer.

3.1 The working principle

The basic design concept is to build a reliable and high-speed measurement system for characterizing the longitudinal and radial magnetic field components, and to determine the integrated field and the magnetic axis from the measurement data.
The basic idea of the method is to induce a voltage in a coil translating co-axially with the magnetic field of an axisymmetric magnet, according to Faraday's induction law (generator convention):

$$U = -\frac{d\Phi}{dt}, \tag{3.1}$$

where U is the voltage induced on the coil and Φ is the magnetic flux linked by the coil, defined as:

$$\Phi = \int_{\mathcal{A}} \mathbf{B} \cdot \mathbf{n} \, da, \tag{3.2}$$

with $\mathcal{A}$ the surface delimited by the coil, da an infinitesimal element of the surface $\mathcal{A}$ and $\boldsymbol{n}$ the unit vector perpendicular to da.

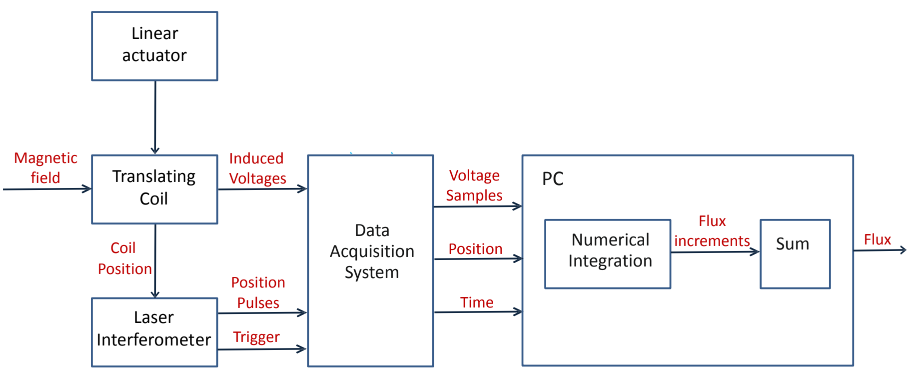

Figure 3.1: Architecture of the translating coil method

Fig. 6.1 shows the architecture of the measurement system. The induction transducer (*translating coil*) is moved by a *linear actuator* coaxially to the magnet. The position is measured by a linear *laser interferometer*, following a retroreflector rigidly connected to the cylindrical core of the transducer. The voltage signal induced at the coil terminal is digitized (*data acquisition*) and integrated between predefined positions along the longitudinal axis of the magnet. The position pulses are sent from the interferometer to the *trigger generator*, where they are counted and used to trigger the *integrator* of the voltage samples to calculate the flux increment between adja-

cent axial positions. In this way, the flux increments are obtained as a function of the linear position. Finally, an adder (Σ) computes the integral flux as a function of the position.
This re-parametrization with respect to the axial position eliminates the time dependence and in particular the influence of linear speed variations, thus relaxing the requirements for the coil transport system. This is the same principle used for the rotating coil measurement method, which uses an angular encoder to obtain the flux as a function of the azimuthal position [1].
The integration can be performed (i) off-line, by acquiring the position pulses and the coil signals by an acquisition device and resorting afterwards to post-processing techniques for the integration, or (ii) on-line, by a digital integrator [57], releasing the value of a flux increment at each trigger signal.

3.2 Induction transducer design

The induction transducer consists of two ideally identical coils, slightly spaced longitudinally (Fig. 3.2). The coils are wound on an accurately-machined cylindrical core, have a diameter of 85 mm and are spaced by 3 mm. The coils are made of a 16-strand copper wire, wound in 16 layers for a total of 256 turns per coil. The total effective area is thus nominally 2.6 m^2. When the two coils are connected in series, they oper-

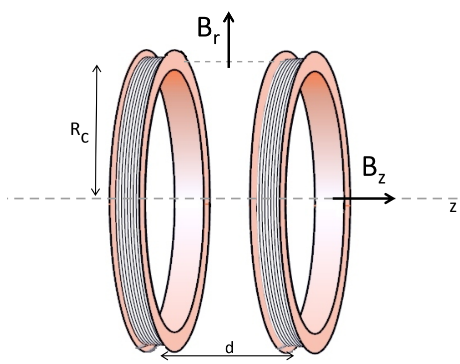

Figure 3.2: The induction transducer with two co-axial sensing coils.

ate like a single coil but with double number of turns. In this case, the transducer is sensitive to the longitudinal component B_z of the field. On the other hand, when the

coils are connected in opposite polarity, the longitudinal component is compensated and the radial component B_r is measured.
The coil diameter has to include the good field region of the magnet where the beam is passing, typically 2/3 of the magnet bore. The voltage in the coil is given by:

$$-U_c = N_T \frac{\partial B_z}{\partial z} v_c A_c$$

where N_T is the number of turns, A_c is the area exposed to flux change for a single turn, $\frac{\partial B_z}{\partial z}$ is the longitudinal field gradient (typically up to 5 T/m in the end region), and v_c is the translating speed along the z-axis (in the range of a few centimeters per second). The number of coil turns is chosen to ensure a nominal peak coil signal about 2 V, which leaves some margin for the effects of vibrations and other mechanical imperfections with respect to the typical ± 5 V input range of the acquisition system. The coil is wound using a flat multi-strand wire [58]. This technique, which requires a skillful manual operation, allows a much more regular cross-section with respect to common automated single-strand winding, leading to easier calibration of the coupling coefficient. A square cross-section, with as many layers as the number of parallel strands in the wire, minimizes non-ideal effects and improves the accuracy of the measurements [59].
The complete transducer is designed to minimize magnetic interferences; in particular, the electrical connections present the smallest area to the changing flux and the coil core is made of a mechanically rigid, non-conductive, and non-magnetic material (Delrin).
The measurement accuracy of the radial field depends strongly on the difference between the effective areas of the two coils. The difference is to be assessed more accurately by calibration, once nominal dimensions and number of turns are defined by design.

3.3 Advantages with respect to Hall-probe measurement systems

The translating coil method is designed in order to allow a direct measurement of the focusing parameters in cylindrically-symmetric magnets. The measurement of the integrated field or the gradient field of axisymmetric magnets it is important for particle tracking studies. By designing a custom coil, the translating coil method allows to measure these quantities directly, thereby greatly improving both measurement speed

and precision.
In fact, a single set of measurements (obtainable in few minutes) can yield the field integrals F_1 and F_2. Currently, these parameters are calculated after a 3D Hall-probe mapping of the magnet which is costly and time-consuming.
With respect to standard Hall probes, translating coils have the following major advantages:

- Linear response to the field: The main sources of non-linearity in a Hall device are due to the geometric factor, the material, and the variation of temperature. As a consequence, Hall probe systems require an elaborate calibration of sensitivity for each probe. On the other hand a fluxmeter presents an inherent linearity between intensity of magnetic field and output signal.

- Temperature sensitivity: The number of charge carriers in a semiconductor depends on the temperature, and the sensitivity of a Hall device is therefore strongly temperature dependent. The advantages of using a fluxmeter is that a wide range of operating temperature is permitted for the measuring coil and, due to the low expansion coefficient of the support (typically fiberglass), a negligible temperature-related drift is obtained.

- Easy absolute calibration: The translating coil can be calibrated by the flip-coil method with 10-4 relative precision in an NMR-mapped dipole. On the other hand, Hall probe systems have the problem of the long term calibration drift. As the semiconductor material ages, the offset, nonlinearity and temperature sensitivity all change. This problem can be solved by periodically re-calibrating the device in a reference field, usually a magnet controlled by NMR. This implies that it is needed to remove the sensor and perform a periodic calibration. The mounting system must allow the sensor to be installed reproducibly in the same position and orientation.

- Spatial resolution: It is possible to obtain an arbitrary resolution in the transversal plane, since the field may be computed at any point of interest from the measured harmonic expansion.

- Planar Hall effect: A magnetic field in the plane of the sensor will also generate a small Hall voltage, and this can pose a problem for mapping 3-D fields. In fact, Hall elements often display even higher-order cross-talk terms between the axes, and for high-precision measurements, these effects become significant and must be corrected.

- Offset: Because of geometric and material imperfections, the Hall voltage will almost always be non-zero in a zero field. In the latest generation of devices, spinning-current techniques, whereby the current is injected into each terminal in turn, are used to cancel most of the offset. The problem persists at a lower level.

- Vibrations, sag and backlash of the mechanical arm: When the magnetic field region to be mapped includes the fringe field and a large mechanical arm is needed, it can be quite challenging to minimize unwanted vibrations and to compensate the related error.

Fluxmeter mapping systems can be of great precision, on the order of 10^{-5}. In fact, they often give results that are clearly superior to those of Hall mappers.
As described above, a single set of measurements can yield a map with arbitrary spatial resolution in the longitudinal direction, as long as we can get all the partial integrals.
On the other hand, the translating coil method is more complex to be used and the equipment is more expensive.

Chapter 4

Proof-of-principle demonstration

At this stage of the project. the basic concept underlying the translating-coils method is to be proved experimentally. For this purpose, a preliminary measurement setup was designed and constructed.

In the following, an experimental proof-of-principle demonstration of the translating-coils method on a solenoid magnet is presented. In particular, (i) the measurement setup, (ii) the induction transducer calibration, and (iii) the validation results are illustrated.

4.1 Measurement setup

The layout of the measurement setup is illustrated in Fig. 5.1. The solenoid under

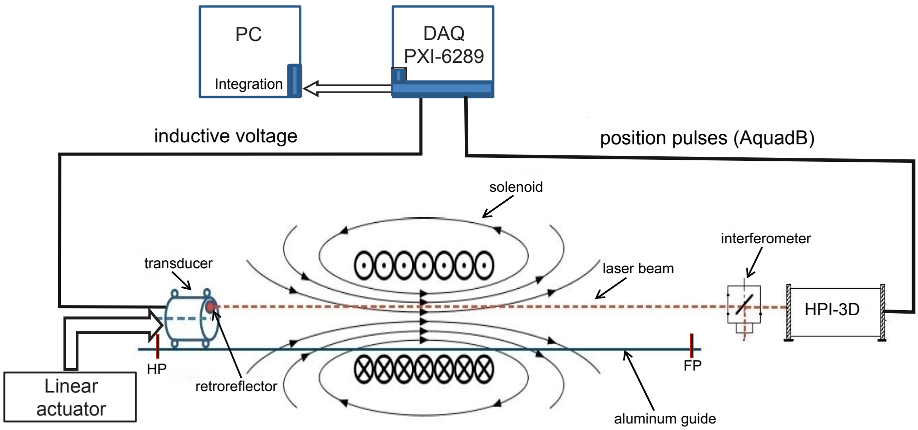

Figure 4.1: Layout of the measurement setup (HP: home position, FP: final position).

test is the spare magnet SNW 200 at CERN, with a coil of 280 turns of resistance 0.0841 Ω, a length of 275 mm, a radius of 65 mm, and with a transfer function in the center of the solenoid $k = B_0/I = 0.0012$ T/A.
A linear actuator pushes and pulls the transducer inside an aluminum guide. The voltage signals induced at the terminals of the two coils are acquired by a data acquisition card (DAQ) NI PXI-6289 [60]. In particular, the voltage signal resulting from the series or anti-series combinations of the two coils is recorded. Synchronously, the coil position measured by a laser interferometer is acquired. The interferometer is fixed outside the aluminum guide and the retroreflector is attached to the coil core (Fig. 5.1). The relative linear motion between the optical components is detected. A digital A-Quad-B signal in 5 V CMOS standard is available on the output of the HPI-3D. The position pulses are acquired and counted by the Data Acquisition System Timing Controller (DAQ-STC), which integrates the counter/timer functionality of the DAQ. When the transducer hits the home position on the longitudinal axis (HP in Fig. 3.2), a LabVIEW software simultaneously stores the position, the inductive voltage, and the time duration within each acquisition step. The voltage samples, yielding the flux increment between adjacent linear positions, are integrated numerically in Matlab.

4.1.1 Translation and position measurement systems

In addition to the induction transducer, the two other fundamental parts of the measurement setup are: (i) the *translation system*, and (ii) the *position measurement* system. The *translation system* includes an aluminum guide, which can be cen-

Figure 4.2: View of the transport system.

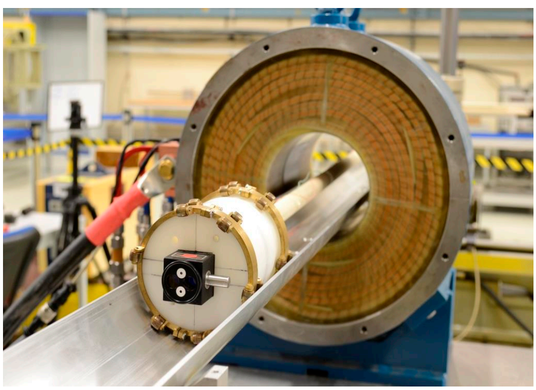

Figure 4.3: Aluminum guide with the rollers for the displacement of the transducer along the longitudinal axis.

tered in the magnet aperture, together with a linear actuator (Fig. 7.1a) for moving the transducer along the longitudinal axis. The transducer moves on non-magnetic rollers, mounted as shown in Fig. 7.1b. The actuator is an external moving system mechanically linked to the coil by a fiberglass stick. It pushes and pulls the transducer from an initial to a final position, such as to cover the entire field of the magnet, including the fringe field.

The linear *position measurement* has a direct impact on the overall system's accuracy. Therefore, special attention was paid to its quality by using a high-performance, heterodyne laser interferometer HPI-3D from Lasertex [61] (Fig. 4.4). The device

Figure 4.4: Laser head and linear interferometer (LI) and retroreflector (LR) for the position measurement.

operates according to the laser interferometer principle and is able to measure objects moving with speeds up to 7 m/s with a nominal resolution of 0.1 nm. The linear optics, consisting of a interferometer and a retroreflector, is employed for precise recording of the induction transducer displacement. The laser beam, generated in the laser head, consists of two polarizations: horizontal and vertical. The linear interferometer (LI in Fig. 4.4) splits the beam into two parts. The horizontally polarized beam is reflected back to the laser head and the vertical polarized beam is directed to the linear retroreflector (LR), which is attached to the translating transducer (Fig. 7.1b). The frequency of the vertical beam varies according to the Doppler effect when the retroreflector is in motion.

4.2 Induction transducer calibration

Another key factor for the proof-of principle demonstration of the translating coil method is the transducer calibration. In the following, the calibration of (i) the *magnetic equivalent area*, and (ii) the *distance* are illustrated.

4.2.1 Magnetic equivalent area

The simplest method of calibration of induction coils is based on moving the coil in a known reference field B_{ref} and directly measuring the magnetic flux Φ resulting from the integration of the coil voltage.
In this case, the total area of the coils is obtained by flipping them upside down in a reference dipole magnet. A second flip, back to the original position, is necessary to evaluate and correct the error due to the integrator drift [?]. Tab. 7.1 shows the calibration results for the two coils mounted on the induction transducer.

Coil	B_{ref}	$\Delta\Phi$	Effective area	R
n.	(T)	(Vs)	(m^2)	(Ω)
1	0.99991	2.66360	1.33171±0.00063	315.4
2	0.99991	2.66271	1.33126±0.00063	315.1

Table 4.1: Calibration results for the translating coils

The measurement of the coil resistance R allows (i) broken coils to be detected, (ii) the number of turns (1%) to be assessed in order to exclude inter-turn shorts, and (ii) load error and impedance mismatch to be corrected.
The difference between the two coils' areas is also an important parameter for assessing the accuracy of the transducer based on the differential principle in radial field measurement. The coils' areas differ by about 0.03%.

4.2.2 Longitudinal coil distance

An accurate calibration of the distance between the two coils of the induction transducer is essential for the correct measurement of the radial component of the magnetic field. Mechanical measurements are usually not possible, since the individual turns cannot be seen by optical instruments or touched by feelers.
Much better results can be achieved by an in-situ magnetic calibration [62]. The longitudinal distance between the two coils is assessed by directly exploiting the magnetic field measurements on the magnet under test. The longitudinal profile of the solenoid magnet is measured independently by the two coils mounted on the induction transducer. Simultaneously, the transducer position is recorded, by associating each element of the measurement arrays with a corresponding position along the longitudinal axis. When the resulting arrays B_{z1} and B_{z2} are plotted as a function of the longitudinal position z (Fig. 4.5), the two curves are slightly spaced by Δz, as highlighted by the zoom in Fig. 4.6. Considering that: (i) the solenoid magnet is

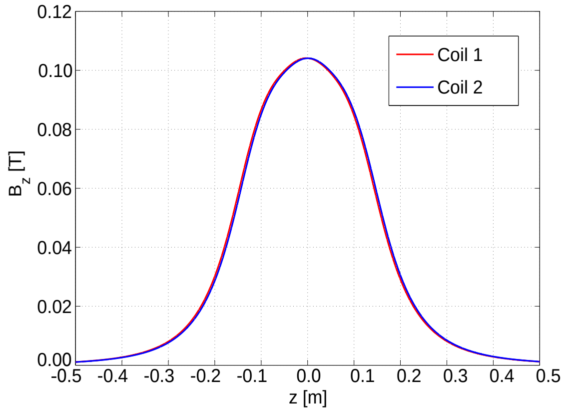

Figure 4.5: Longitudinal magnetic field measured independently and simultaneously by the two coils.

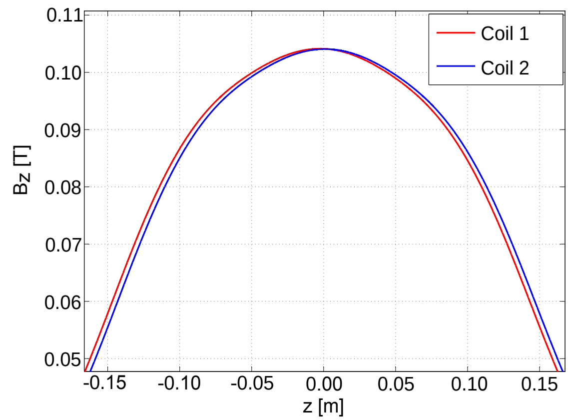

Figure 4.6: Zoom in z=[-0.15, 0.15] to highlight the coil distance effect.

powered with a stable DC current, (ii) the coils are designed to be identical and are coaxially mounted on the core of the induction transducer, and (iii) the measurements are carried out independently and simultaneously by the two coils, the offset Δz between the longitudinal profiles measured by the two coils is assumed as due to the longitudinal distance between the two coils.

Ideally, the value Δz should be the same for each pair of corresponding points $(B_1(j), B_2(j))$ of the two curves. Considering that the measurements are affected by several error sources, there is a variation of Δz for each pair of points as shown in Fig. 4.7. Therefore, the calibration procedure for the distance consists in determining the value of Δz that minimizes the Euclidean distance between the vectors B_1 and

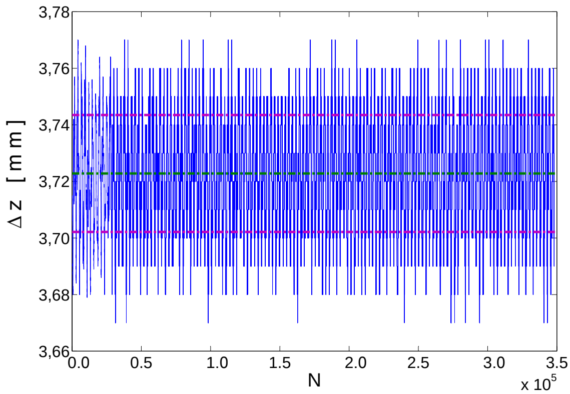

Figure 4.7: Absolute difference for each pair of corresponding points $(B_1(j), B_2(j))$ of the two coils measurements (mean: green, 1-sigma: magenta).

B_2:

$$\min_{\Delta z} \parallel B_2(z) - B_1(z) \parallel \tag{4.1}$$

For the prototype, the calibrated longitudinal distance between the two coils is given by the mean difference of all the points, $\Delta z = 3.723 \pm 0.021$ mm.

4.3 Validation results

The translating coil method was validated experimentally in comparison to a 3D Hall probe mapper available at CERN.

The magnetic field of the same cylindrical region inside the solenoid aperture was measured by both methods. This region is delimited longitudinally, by the maximum displacement of the mapping system along the axis of the solenoid, and transversally by the coils' windings.

In Fig. 4.8, the results of the translating coil method and Hall probe mapping are compared for the longitudinal magnetic field. In Fig. 4.9, the absolute differences are plotted. An analogous comparison is reported in Figs. 4.10 and 4.11 for the radial field. These differences are compatible with the accuracy of the absolute calibration and the positioning of the Hall probe system. The impact of the mechanical precision of the movement of the translating coil in terms of tilt angle and offset, remains to be assessed.

The normalized root-mean-square error (NRMSE) is 0.14% for the longitudinal component of the magnetic field B_z and 0.85% for the radial component B_r. The Lar-

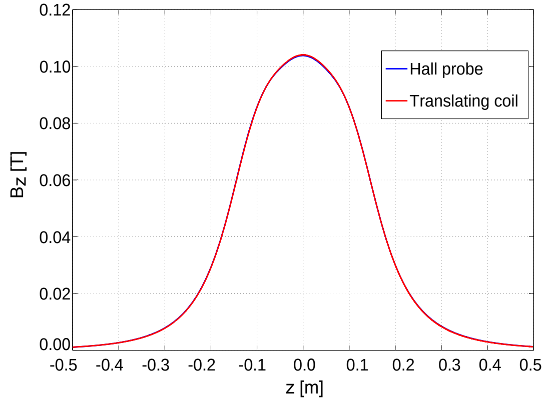

Figure 4.8: Comparison between translating coil method and reference Hall probe mapping: longitudinal magnetic field.

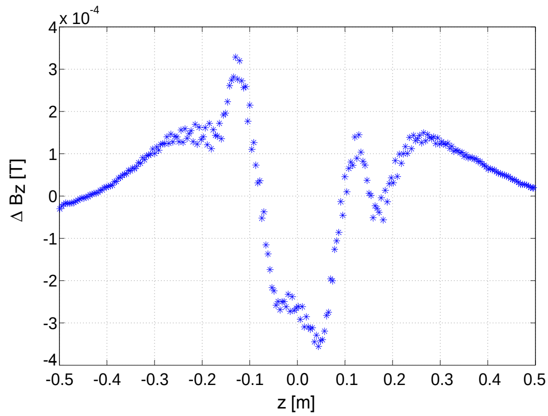

Figure 4.9: Absolute differences.

mor angle and the focusing strength for the solenoid under test can be easily evaluated from the measurement data. The field integrals provided by the solenoid are $F_1 = 0.0359$ Tm and $F_2 = 0.0027$ T^2m.

4.4 Discussion

A method based on translating coils for the magnetic field measurement of axially-symmetric magnets has been proposed. An induction transducer, sensitive to the longitudinal and radial field components, was designed and constructed. The effec-

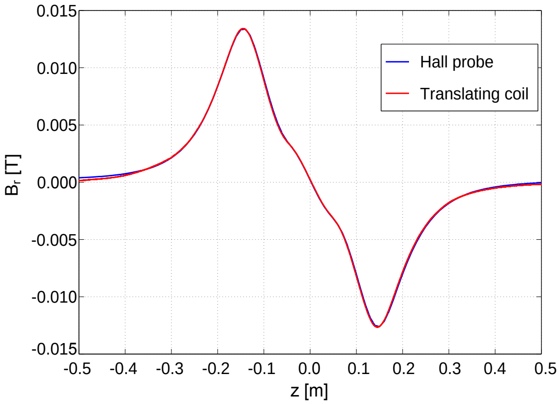

Figure 4.10: Comparison between translating coil method and reference Hall probe mapping: radial magnetic field.

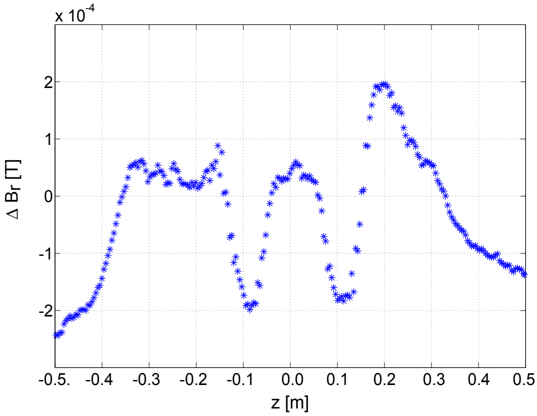

Figure 4.11: Absolute differences.

tive surface of the coils and the longitudinal distance between them were calibrated. The radial and longitudinal components of a CERN solenoid measured by the proposed method were compared to a reference measurement method with satisfying agreement. Furthermore, from the measurement data, the field integrals F_1 and F_2 were evaluated.
The required accuracy of the prototype still needs improvements on the mechanics and calibrations of the individual parts in order to achieve adequate metrological performance. A reference (calibrated) solenoid is required for the metrological characterization of the translating-coil system. The uncertainty analysis of the measurement

system and an optimization of the induction transducer are crucial as the technical realization of a better transport system. Theoretical studies for the reconstruction of 3D magnetic fields from the measurement data will have to be carried out to further advance the assessment of the local field.

Chapter 5

Uncertainty analysis

In the uncertainty assessment of magnetic flux measurements in axially symmetric magnets by the translating coil method, the Guide to the Uncertainty in Measurement and its supplement cannot be applied: the voltage variation at the coil terminals, which is the actual measured quantity, affects the flux estimate and its uncertainty. In this Chapter, a particle filter, implementing a Sequential Monte-Carlo method based on Bayesian inference, is applied. At this aim, the main uncertainty sources are analyzed and a model of the measurement process is defined. The results of the experimental validation point out the transport system as the main contribution to the uncertainty budget.

5.1 Introduction

The characterization of the magnetic field of axially-symmetric (*axisymmetric*) magnets is paramount for focusing systems in the low-energy section of accelerators [2] and other devices, such as electron microscopes [3], or electron guns. Other meaningful applications are related to systems for laser-accelerated protons or ions [5]. Examples are particle therapy and short-pulse radio-graphic diagnostics, where axisymmetric magnets are useful for effective focusing and energy selection.

The needed focusing strength imposes strict requirements to the magnetic field measurement and axis determination. Traditional general-purpose techniques, as 3D Hall probe mapping systems [9], are poorly suitable to exploit the inherent symmetry of axisymmetric magnets. Analogously, available state-of-the-art stretched– [11] and vibrating-wire [12] systems provide information only about integral field properties. Conversely, an investigation on the local field geometrical parameters and the field homogeneity is also important for the full characterization of axisymmetric magnets.

In [14], an alternative measurement method, conceived expressly to exploit the inherent axial symmetry of the magnetic field, was proposed. The magnetic flux, linked with a pair of sensing coils translating co-axially to the magnet, is measured as a function of the longitudinal position. Then, a suitable model based on cylindrical symmetry is exploited to map the local field geometrical parameters and to measure the field integral. With respect to standard Hall-probe mapping, the method has several advantages: (*i*) inherent linearity, (*ii*) negligible thermal drift, owing to the low expansion coefficient of the support (typically fiberglass), (*iii*) easy calibration, by flipping the sensing coils in a reference magnet, and (*iv*) better resolution in the transverse plane, because the field can be computed at any point of interest from the harmonic expansion of the measured field.

Nevertheless, after the successful proof-of-principle demonstration of the translating coils method [14] at CERN, the high-level metrological target of potential applications requires several improvements to the mechanics, as well as calibrations of the individual parts of the system. Moreover, an uncertainty analysis is necessary for a comprehensive metrological characterization of the method.

At this aim, the uncertainty sources affecting the measurement system have to be evaluated and their influence on the result assessed. A measurement model, relating the output (measurand) y to the input quantities $x_1, ..., x_N$, is to be formalized, by assigning the probability distributions to the input quantities on the basis of available knowledge. Then, the probability distributions of the x_i need to be propagated through the measurement model $y = f(x_1, ..., x_N)$ in order to obtain the probability distribution of the output quantity.

In literature, the approaches to the propagation of distributions can be grouped in three main categories [63]: (*i*) the GUM (Guide to the expression of the Uncertainty in Measurement) framework [64], where the law of uncertainty propagation is used, (*ii*) analytical methods, where an algebraic form of the probability distribution is derived by mathematical analysis, and (*iii*) Monte–Carlo methods [65], where an approximation of the probability distribution of the output is found numerically by starting from those of the input quantities. The GUM approach follows a general approximation, not applicable to nonlinear measurement models or non-Gaussian distributions. Analytical methods give exact and complete solutions, but for complex measurement models they are often hard to define in a closed form. Finally, Monte–

Carlo methods offer a practical solution when both the GUM approach and analytical models are not applicable.

However, both the GUM framework and the Monte–Carlo approach described in [65] assume the measurand to be constant, and therefore are not appropriate for translating coils, where the measurands depend on continuous variables [66]. In particular, in this case, referred to as *dynamic measurement*, the measurand variation (e.g., in time or space domain) has a significant effect on the estimate of the measurand and the associated uncertainty [67].

Recently, Sequential Monte–Carlo (SMC) methods have been proposed, allowing dynamical changes in the input distributions to be tracked, thus adapting themselves automatically to provide the dynamic distribution of the output. Sequential Monte–Carlo methods represent a memory-efficient alternative to traditional Monte–Carlo methods for dynamic measurements, because although the results are identical, the output values are stored only for a small number of time instants [68]. Moreover, with respect to Unscented Kalman filters, they allow to completely describe the distribution of the system state, in the case of non-linear systems.

In this chapter, the measurement model for the translating coil method is formulated and an SMC algorithm, based on Bayesian inference, is then used to dynamically estimate the distribution of the output quantity, starting from the knowledge of the distributions of all the uncertainty sources considered in the model. In particular, in Section 5.2 the translating coil method proposed in chapter 3 is outlined. In Section 5.3, the sources of uncertainties are analyzed and assessed, by investigating experimentally and numerically the predominating source, the transport system. Then, in Section 5.4, the measurement model is defined, by listing and discussing all the considered uncertainty sources. In Section 5.5, the SMC–based algorithm for uncertainty propagation is described. Finally, the experimental results of the characterization of the uncertainty sources are reported in Section 5.6.

5.2 Translating coils background

Main design requirements are (*i*) to build a reliable and high-speed measurement system for characterizing the longitudinal and radial magnetic field components of axisymmetric magnets, as well as (*ii*) to measure the integrated field and locate the magnetic axis.

The working principle of the method is to induce a voltage in a coil translating coaxially with the magnetic field of an axisymmetric magnet, according to the Faraday's

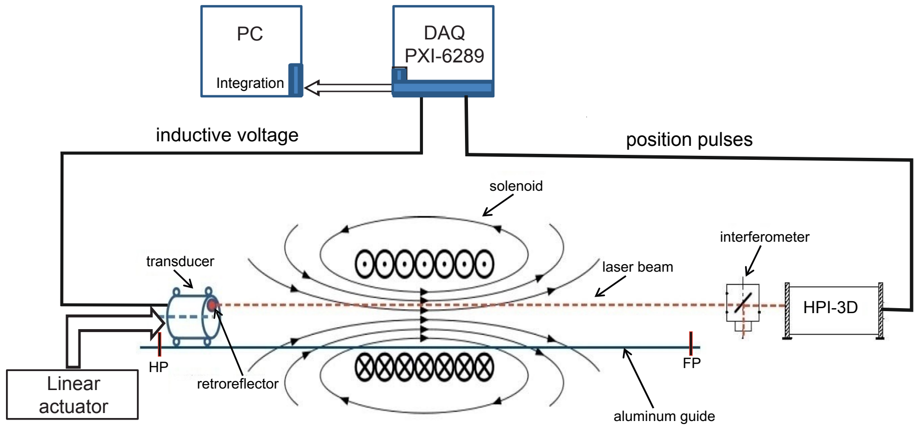

Figure 5.1: Layout of the measurement set-up (HP: home position, FP: final position) [12].

induction law (generator convention):

$$U = -\frac{d\Phi}{dt}, \tag{5.1}$$

where U is the voltage induced on the coil and Φ is the magnetic flux linked by the coil, defined as:

$$\Phi = \int_{\mathcal{A}} \mathbf{B} \cdot \mathbf{n} \, da, \tag{5.2}$$

with $\mathcal{A}$ the surface delimited by the coil, da an infinitesimal element of the surface $\mathcal{A}$ and $\boldsymbol{n}$ the unit vector perpendicular to da.

The measurement set-up, designed and constructed for a proof-of-principle demonstration is shown in Fig. 5.1. A transducer hosting two coils is moved by a linear actuator along an aluminum guide. The voltages induced at the coils terminals are acquired by a data acquisition card NI PXI-6289 (DAQ) [60]. In particular, the resulting voltage arising from the series and anti-series combination of the two coils is recorded. Simultaneously, also the longitudinal position of the coils is acquired by means of a laser interferometer system HPI-3D from Lasertex. The position pulses output by the interferometer are acquired and counted by a data acquisition system timing controller (DAQ-STC). When the transducer hits the home position on the longitudinal axis (HP in Fig. 5.1), a program in LabVIEW® simultaneously stores the position, the inductive voltage, and the time duration within each acquisition step. The voltage samples, yielding the flux increment between adjacent linear positions,

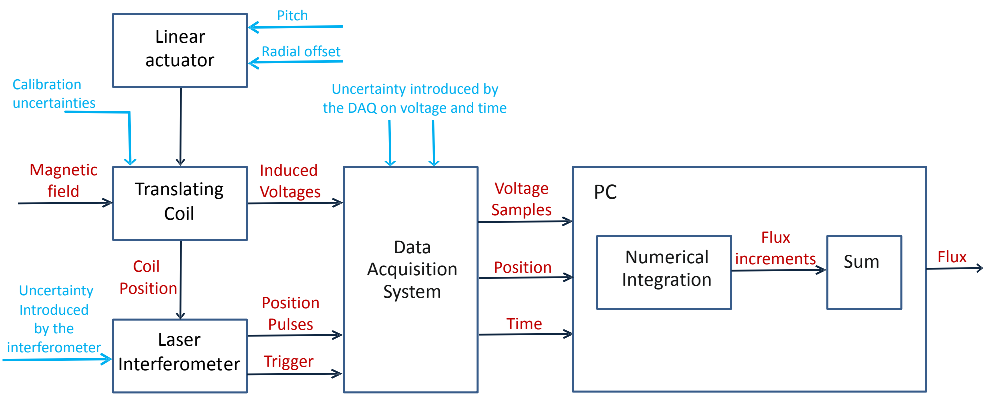

Figure 5.2: Architecture of the translating coils method with the measurement quantities (red) and the main uncertainty sources (light blue).

are integrated numerically in MATLAB®.

5.3 Uncertainty sources

In Fig. 5.2, the measurand, the intermediate quantities, and the output are highlighted in red inside the architecture of the translating coils method, while the uncertainty sources, introduced either intrinsically by the method or by the measurement instruments, in blue. In the following, the uncertainty sources are analyzed.

5.3.1 Data acquisition

The acquisition system measures the voltage signals induced in the sensing coils and counts the rising edges of the position pulses coming from the interferometer. Therefore, the uncertainty on these two quantities must be taken into account. In addition to the DAQ uncertainty, the voltage measurements are affected by random noise. The resulting uncertainty was assessed by a test acquisition without applying the input signal, in the same working conditions used during the actual signal acquisition. This test resulted in an uncertainty of 210 µV. The time measurement uncertainty is determined by the time resolution. Considering a sampling rate of 10 kSamples/s, it is equal to 100 µs.

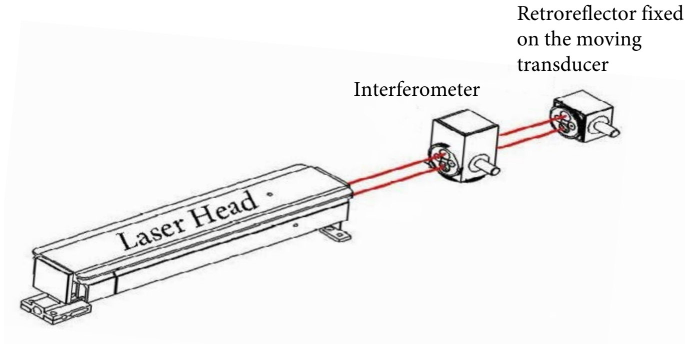

Figure 5.3: Laser interferometer system: the laser head and the interferometer are fixed outside the measurement path and the retroreflector moves with the transducer.

5.3.2 Position measurement

Another source of uncertainty is the position of the transducer along the measurement path. The linear position measurement has a direct impact on the overall system's metrological performance. Therefore, a high-performance heterodyne laser interferometer was used to measure the linear position. A quadrature encoder signal is produced as output, where the pulse number indicates the relative distance between retroreflector and interferometer (Fig. 5.3). These signals are given in input to a counter that counts the low to high transitions in the waveform and emits a corresponding value, finally converted to position according to the used encoding. The resolution on the position depends on the interferometer distance owing to the range variation: 10 µm or 100 µm, for less or more than 1 m, respectively.

5.3.3 Coils fabrication

A geometrical uncertainty arises from the tolerances of the absolute position of the sensing coils and from their orientation inside the transducer core. These two tolerances sum up to a total positioning uncertainty, resulting in a systematic effect on the final result. This effect can be assessed by calibration and its value exploited to correct the measurements.

5.3.4 Transport system

In the proof-of-principle demonstration of the translating-coil method [14], the transducer is assumed to move ideally along the magnet axis. However, the longitudinal movement is realized by means of a linear actuator, connected by a shaft to the transducer. The transducer, equipped with non-magnetic roller bearings, is placed on an aluminium guide (Fig. 5.4). The surface contact between the guide and the roller bearings introduces an oscillatory motion, resulting in off-axis displacements in the radial direction, and tilting of the coils mainly around the X–axis. Both radial displacement and tilt contain random contributions to be considered owing to their contribution to the overall uncertainty. The variation range of such quantities is not known a priori, thus they have to be determined experimentally.

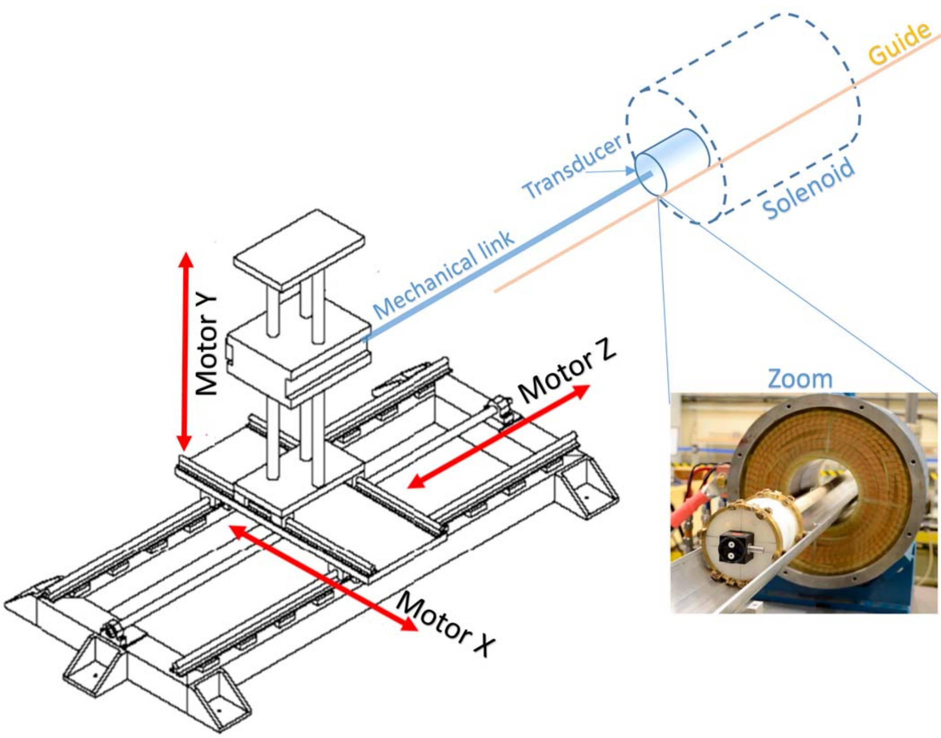

Figure 5.4: The transport system includes a 3D translational table and a rigid mechanical link that moves the inductive transducer inside the solenoid bore. The zoom highlights the contact between the roller bearings and the aluminium guide.

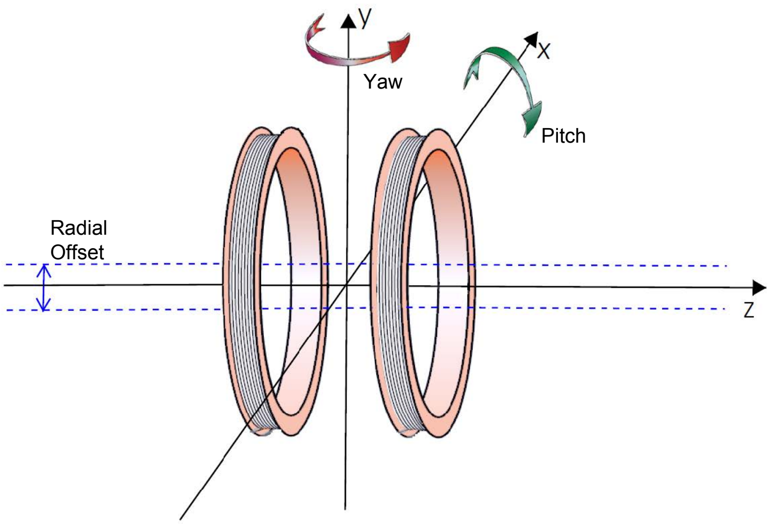

Figure 5.5: Pitch, yaw, and off-axis displacement of the induction transducer, with an overlay of the coordinate axes.

Experimental characterization

A heterodyne laser interferometer (HPI-3D from Lasertex [61]) was used to measure the X-Y displacements and the pitch during the translation of the transducer along the Z-axis. Each measurement was repeated 15 times and the results are plotted in terms of mean and standard deviation in Figs. 5.6 and 5.7, for the displacements along X and Y, respectively. The displacement is more significant along the X-axis, up to a maximum value of 0.6 mm, rather than along the Y-axis.
By substituting the angular optics (both interferometer and retro-reflector) in the HPI-3D, the pitch (Fig. 5.8) and yaw variations (Fig. 5.9) were monitored analogously during the motion. Both X and Y displacements and pitch angle variations follow a determined trend during the translation along the longitudinal axis. It means that these effects have a relevant systematic component, completely related to the quality of the transport system, which can be compensated, thus increasing the accuracy of the result.
Moreover, it can be observed that the variations of the yaw are very small compared to those of the pitch.

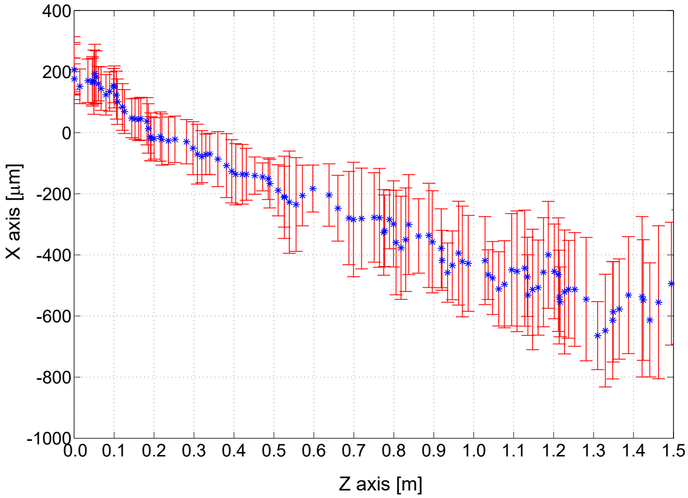

Figure 5.6: Mean (star) and 1-sigma repeatability (error bar) of X-axis variation of the coils during the longitudinal translation over 15 repetitions.

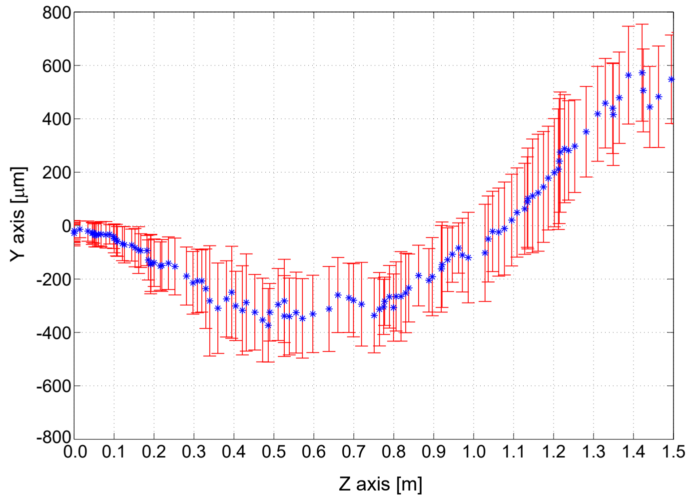

Figure 5.7: Mean (star) and 1-sigma repeatability (error bar) of Y-axis variation of the coils during the longitudinal translation over 15 repetitions.

Transport uncertainty effects on the measured flux

The effects of the transport system uncertainty on the measured flux were evaluated by Monte–Carlo simulations. Owing the field symmetry, the uncertainty of the coil

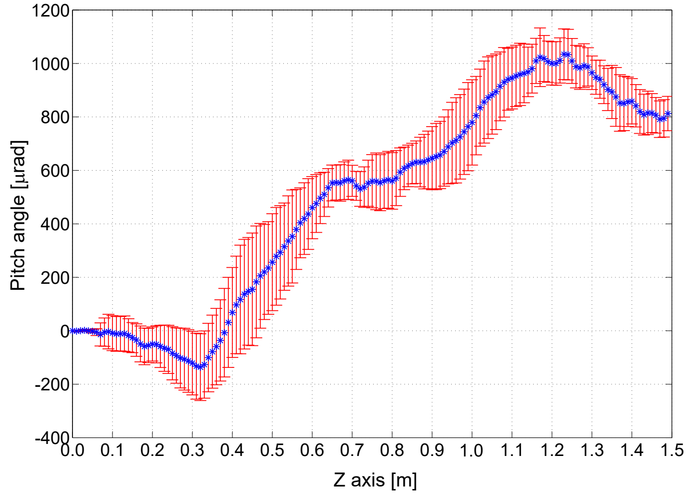

Figure 5.8: Mean (star) and 1-sigma repeatability (error bar) of pitch variation of the coils' orientation during the longitudinal translation over 15 repetitions.

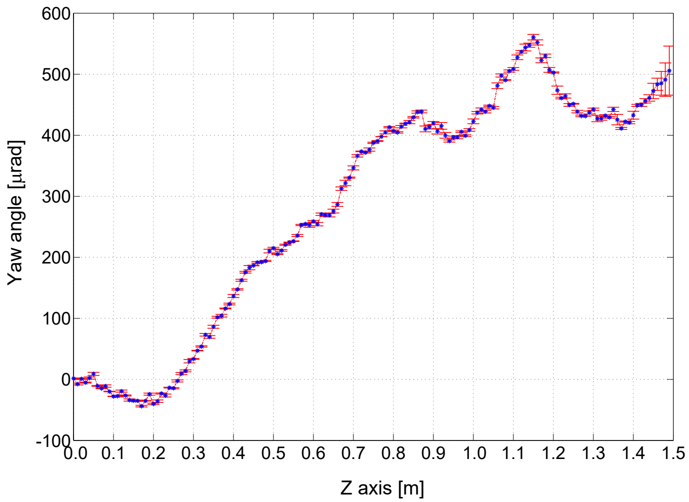

Figure 5.9: Mean (star) and 1-sigma repeatability (error bar) of yaw variation of the coils' orientation during the longitudinal translation over 15 repetitions.

system can be described by the radial offset Δr and the tilt ϑ. In particular, the standard deviation of the radial offset can be determined by combining quadratically the standard deviations of the measured displacements along X and Y and the standard deviation of the tilt can be determined similarly by combining those of the pitch and the yaw. The results are 183 µm for the radial offset and 107 µrad for the tilt. Therefore, Δr and ϑ have been varied along the measurement path with Gaussian distributions that have null means and standard deviations $\sigma_{\Delta r}$ and σ_ϑ, respectively. The flux measured by the coils can be obtained starting from the expressions of the longitudinal and radial components of the magnetic field inside the solenoid. In particular, starting from the Laplace equation for the magnetic scalar potential in 3D cylindrical coordinates, exploiting the cylindrical symmetry of the magnetic field inside the solenoid, and expanding the magnetic scalar potential in Taylor series versus the distance r from the axis, the following expressions is derived [?]:

$$\begin{aligned} B_z(r,z) &= -\mu_0 \left(B_z(0,z) - \frac{B_z^{(2)}(0,z)}{4} r^2 + \frac{B_z^4(0,z)}{64} r^4 \right) \\ B_r(r,z) &= -\mu_0 \left(-\frac{B_z^{(1)}(0,z)}{2} r + \frac{B_z^{(3)}(0,z)}{16} r^3 \right), \end{aligned} \tag{5.3}$$

where, z is the longitudinal position of the coil, $B_z(r,z)$ and $B_r(r,z)$ the longitudinal and radial components of the magnetic field, respectively, and the superscript $^{(n)}$ denotes the n-th derivative. The term $B_z(0,z)$ is the magnetic field on the magnetic axis. Such a term can be obtained from either a characterization of the magnet by a different measurement method, e.g by a Hall probe mapper, as in the case of this work, or by Finite Element Method simulation.

The flux measured by the coil can be derived by integrating the expressions (5.3) on the coil surface, by taking into account the perturbations introduced by the radial displacement and the tilt (Fig. 5.10).

Therefore, the measured flux has the following expression:

$$\begin{aligned} \Phi_m(z) = N \Bigg[&\int_0^R B_z(\Delta r + \rho\cos\vartheta, z + \rho\sin\vartheta)\cos\vartheta \; 2\pi\rho \; d\rho + \\ &+ \int_0^R B_r(\Delta r + \rho\cos\vartheta, z + \rho\sin\vartheta)\sin\vartheta \; 2\pi\rho \; d\rho \Bigg]. \end{aligned} \tag{5.4}$$

where, R is the coil radius and N is the number of turns of the coil.
Considering that the product $\rho\sin\vartheta$ is small and the components of the field are slowly changing with z, the terms $B_z(\Delta r+\rho\cos\vartheta, z+\rho\sin\vartheta)$ and $B_r(\Delta r+\rho\cos\vartheta, z+\rho\sin\vartheta)$ can be approximated with $B_z(\Delta r + \rho\cos\vartheta, z)$ and $B_r(\Delta r + \rho\cos\vartheta, z)$, respectively,

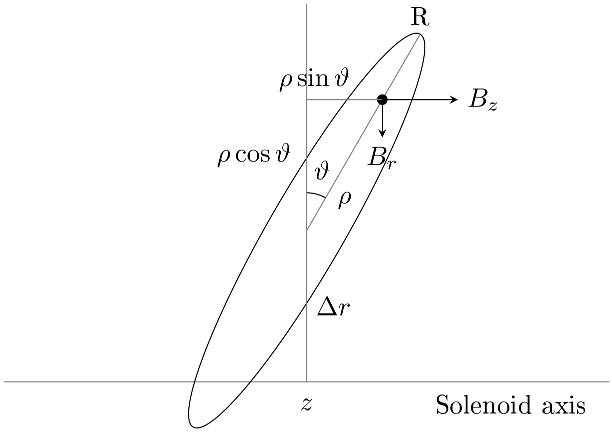

Figure 5.10: Derivation of the flux from the components of the magnetic field.

thus leading to:

$$\begin{aligned}\Phi_m(z) \approx N \Bigg[\int_0^R B_z(\Delta r + \rho\cos\vartheta, z)\cos\vartheta \; 2\pi\rho \; d\rho \; + \\ + \int_0^R B_r(\Delta r + \rho\cos\vartheta, z)\sin\vartheta \; 2\pi\rho \; d\rho \Bigg] .\end{aligned} \tag{5.5}$$

Substituting (5.3) in (5.5), and solving the integral, the following expression is obtained:

$$\Phi_m(z) = 2\pi N \left(\Phi_{B_z}\cos\vartheta + \Phi_{B_r}\sin\vartheta\right), \tag{5.6}$$

where:

$$\begin{aligned}\Phi_{B_z}(z,\vartheta,\Delta r) &= B_z(0,z)\frac{R^2}{2} - \frac{B_z^{(2)}(0,z)}{4}\left[\frac{2}{3}\Delta r\cos\vartheta R^3 + \cos^2\vartheta\frac{R^4}{4}\right] + \\ &+ \frac{B_z^{(4)}(0,z)}{64}\left[\frac{4}{5}\Delta r R^5\cos^3\vartheta + \frac{R^6}{6}\cos^4\vartheta\right], \\ \Phi_{B_r}(z,\vartheta,\Delta r) &= -\frac{B_z^{(1)}(0,z)}{2}\left[\Delta r\frac{R^2}{2} + \cos\vartheta\frac{R^3}{3}\right] + \\ &+ \frac{B_z^{(3)}(0,z)}{16}\left[\frac{3}{4}\Delta r\cos\vartheta\frac{R^4}{4} + \cos^3\vartheta\frac{R^5}{5}\right].\end{aligned} \tag{5.7}$$

In Figs. 5.11, the results of the simulation analysis are shown. In particular, the difference of the actual magnetic flux computed through (5.6) and (5.7) and the ideal one has been assessed. For the case of equation (5.6) (Fig.5.11a), only the coil tilt has been applied, with a standard deviation $\sigma_\vartheta = 107\,\mu\text{rad}$. In the latter case, only the radial displacement has been applied, with a standard deviation of $\sigma_{\Delta r} = 183\,\mu\text{m}$. The radial displacement has a greater impact on the measured magnetic flux, giving errors of an order of magnitude higher than the tilt. Moreover, by observing the shape of the error, in the case of the pitch, a greater contribution to the error is given by the radial component of the field. In the case of the radial displacement, instead, the higher contribution to the error is given by the longitudinal field.

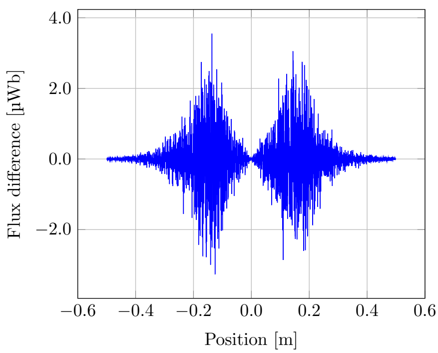

(a) $\sigma_\vartheta = 107\,\mu\text{rad}$, $\sigma_{\Delta r} = 0$

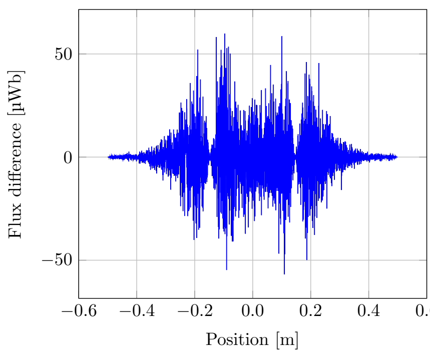

(b) $\sigma_\vartheta = 0$, $\sigma_{\Delta r} = 183\,\mu\text{m}$

Figure 5.11: Effects on the measured magnetic flux of the coil pitch (a) and the radial displacement (b).

5.3.5 Discussion

As a result of the uncertainty analysis, a summary of the uncertainty sources with their values is reported in Tab. 7.1.

As mentioned above, the uncertainty of the position measurement system is determined by its resolution, equal to $10\,\mu\text{m}$ and $100\,\mu\text{m}$ for distances lower and higher than $0.181\,\text{m}$, respectively.

The transport system contributes to the uncertainty budget with the radial offset and the tilt, whose standard deviation have been determined as $183\,\mu\text{m}$ and $107\,\mu\text{rad}$, respectively.

For the acquisition system, the uncertainty of the voltage measurement, determined by a preliminary test, resulted equal to $210\,\mu\text{V}$, while that of time base is determined by the sampling period equal to $100\,\mu\text{s}$.

The uncertainties related to the calibration of the distance between coils and their surface are also reported. The calibration of the coils orientation is currently under investigation.

It is worth noting, finally, that in the conducted analysis, only the random uncertainty sources have been considered. However, some systematic effects can arise. Most of all, the measured voltage can depend on a deviation both in displacement and orientation of the coil trajectory from the magnetic axis. For minimizing such deviation, a preliminary phase including fiducialization and magnetic axis determination of the solenoid under test has been carried out at CERN [69].

System	**Uncertainty source**	**Uncertainty**
Position measurement system	Laser interferometer HPI-3D	10 µm or 100 µm
Transport system	Radial displacement of the coil system	183 µm
	Pitching of the coil system	107 µrad
Acquisition system	DAQ accuracy in measuring the induced voltage	210 µV
	Time base	100 µs
Calibration	Surface calibration	1×10^{-4} T
	Distance calibration	1×10^{-4} T
	Orientation of the coils	To be evaluated

Table 5.1: Main uncertainty sources in the translating-coil system. The calibration of the coils orientation is currently under investigation.

5.4 Measurement process model

In the translating-coil method, the magnetic flux is measured indirectly from the voltage induced on the coil. The measurement process can be modeled as a discrete-time system (Fig. 5.12), generating samples of the longitudinal position of the transducer $z(k)$ and the coil voltage $u(k)$, at each sampling instant t_k. The magnetic flux is a hidden internal state of the system that cannot be measured directly. Therefore, an observation process is needed also, which receives as input the measured quantities and estimates the hidden state of the measurement process.

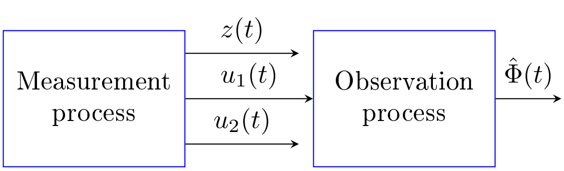

Figure 5.12: Block diagram of the translating-coil measurement process modeled as a discrete-time system.

The behavior of the measurement process can be described by first analyzing the movement of the coils, when the sampling events occur. In particular, in order to model the movement of the coil, a *discrete-time (nearly) constant velocity* model has been applied, which is commonly used as a priori model in data fusion algorithms for target tracking applications [70]. Such model represents a discretized version of a continuous time model, where the acceleration is a null mean Gaussian process with a variance σ_a^2 and is described by the following matrix equation:

$$\begin{bmatrix} z(k) \\ s(k) \end{bmatrix} = \begin{bmatrix} 1 & T \\ 0 & 1 \end{bmatrix} \begin{bmatrix} z(k-1) \\ s(k-1) \end{bmatrix} + \mathbf{v}_m(k-1) \tag{5.8}$$

where, T is the sampling period and $\mathbf{v}_m(k-1) = \begin{bmatrix} v_z(k-1) & v_s(k-1) \end{bmatrix}^T$ is a bivariate Gaussian random process with null mean and covariance matrix:

$$\mathbf{Q} = \sigma_a^2 \begin{bmatrix} T^3/3 & T^2/2 \\ T^2/2 & T \end{bmatrix}. \tag{5.9}$$

As shown in Section 5.3.4, the magnetic flux sensed by each coil can be assessed from the magnetic field inside the solenoid, as function of the coil tilt and the radial displacement, by applying (5.6) and (5.7). Thus, the magnetic fluxes measured by the coils are:

$$\begin{aligned} \Phi_1(k) &= N_1 \cdot F(z(k-1), \vartheta(k-1), \Delta r(k-1)) \\ \Phi_2(k) &= N_2 \cdot F(z(k-1) + d, \vartheta(k-1), \Delta r(k-1)) \end{aligned} \tag{5.10}$$

with:

$$F(z, \vartheta, \Delta r) = 2\pi \left[\Phi_{B_z}(z, \vartheta, \Delta r) \cos\vartheta + \Phi_{B_r}(z, \vartheta, \Delta r) \sin\vartheta\right] \tag{5.11}$$

where d is the distance between the coils and N_1 and N_2 are the turns of the first and the second coil, respectively.

The outputs of the measurement processes are the position measurement and the voltage induced on each coil, that can be modeled by the following equations, where the uncertainties introduced by the measurement instruments on the position measurement z_m and on the voltage measurements $u_{1,m}$ and $u_{2,m}$ have been modeled:

$$\begin{aligned} z_m(k) &= z(k) + w_z(k) \\ u_1(k) &= -\frac{\Phi_1(k) - \Phi_1(k-1)}{T} + w_{u_1}(k) \\ u_2(k) &= -\frac{\Phi_2(k) - \Phi_2(k-1)}{T} + w_{u_2}(k) \end{aligned} \tag{5.12}$$

In (5.12), $w_z(k)$ takes into account the uncertainty on the position measurement, introduced by the interferometer, and w_{u_1} and w_{u_2} consider the uncertainty on the voltage measurement introduced by the data acquisition.

$w_z(k)$ is modeled as a uniform random variable $w_z(k) \sim U(-e_i(z), e_i(z))$, with $e_i(z)$ the uncertainty of the interferometer at position z. Similarly, w_{u_1} and w_{u_2} are modeled as uniform random variables, $w_{u_1}, w_{u_2} \sim U(-e_u, e_u)$, with e_u the uncertainty of the data acquisition.

5.5 Observation process based on Bayesian inference

The above model of the measurement process has the following characteristics:

(i) non-linear, because the magnetic flux depends non-linearly on the longitudinal position $z(k)$ and on the coils pitch ϑ;

(ii) time-variant error terms, e.g. the position measurement error, depending on the distance, which in turn increases with time;

(iii) non-Gaussian error terms, e.g. for the position measurement, where the uncertainty is determined by the resolution. Therefore, since all the instants inside the resolution interval are equally probable, the error is better modeled by a uniform distribution.

Therefore, a Sequential Monte Carlo (SMC) approach has been chosen for the observation process. In particular, an Auxiliary Sequential Importance Resampling (ASIR) particle filter has been used [71]. In the following subsections, first some theoretical details about the particle filter are given. Then, the design of the observer process, by means of the particle filter, is described.

5.5.1 The particle filter

Let's consider a discrete-time dynamic system, whose state is represented by the vector $\mathbf{x}(k)$ and with outputs $\mathbf{y}(k)$, where $\mathbf{x}(k)$ cannot be measured directly, and let the system be described by the following equations:

$$\begin{aligned} \mathbf{x}(k) &= f_k(\mathbf{x}(k-1), \mathbf{v}(k-1)) \\ \mathbf{y}(k) &= h_k(\mathbf{x}(k), \mathbf{w}(k)) \end{aligned} \tag{5.13}$$

where f_k and h_k are nonlinear functions, $\mathbf{v}(k-1)$ is an i.i.d. process noise sequence, and $\mathbf{w}(k)$ is an i.i.d. measurement noise sequence.

The objective of the particle filter is to estimate the hidden state $\mathbf{x}(k)$ recursively, as measurement $\mathbf{y}(k)$ becomes available. At each sampling time, a complete solution is assessed, consisting of the conditional posterior density $p(\mathbf{x}(k)|\mathbf{y}(1), \ldots, \mathbf{y}(k))$ of the state $\mathbf{x}(k)$, taking all observations $\{\mathbf{y}(1), \mathbf{y}(2), \ldots, \mathbf{y}(k)\}$ into account. By knowing the conditional posterior density, the state can be estimated, for example by computing the conditional expectation:

$$\hat{\mathbf{x}}(k) = \int \mathbf{x}(k) \cdot p(\mathbf{x}(k)|\mathbf{y}(1) \ldots \mathbf{y}(k)) \; d\mathbf{x}(k). \tag{5.14}$$

Other estimates, such as the median or the mode can also be obtained from the conditional posterior density.

The computation of the conditional posterior density requires the computation of all measurements $\mathbf{y}(1), \ldots, \mathbf{y}(k)$ in a single sampling time. However, the posterior density can be updated recursively with the new measurements:

$$\begin{aligned} p(\mathbf{x}(k)|\mathbf{y}(1) \ldots \mathbf{y}(k)) &= \frac{p(\mathbf{y}(1) \ldots \mathbf{y}(k)|\mathbf{x}(k))p(\mathbf{x}(k))}{p(\mathbf{y}(1) \ldots \mathbf{y}(k))} = \\ &= \frac{p(\mathbf{y}(k)|\mathbf{x}(k))p(\mathbf{x}(k)|\mathbf{y}(1) \ldots \mathbf{y}(k-1))}{p(\mathbf{y}(k)|\mathbf{y}(1) \ldots \mathbf{y}(k-1))}. \end{aligned} \tag{5.15}$$

The recursive computation of the posterior density is organized in two steps: *(i) prediction* and *(ii) update*.

In the *prediction*, the prior density at the sampling time k is obtained by using the posterior density at the previous sampling time $k-1$:

$$p(\mathbf{x}(k)|\mathbf{y}(1) \ldots \mathbf{y}(k-1)) = \int p(\mathbf{x}(k)|\mathbf{x}(k-1))p(\mathbf{x}(k-1)|\mathbf{y}(1) \ldots \mathbf{y}(k-1))d\mathbf{x}(k-1), \tag{5.16}$$

where the state transition density $p(\mathbf{x}(k)|\mathbf{x}(k-1))$ depends on the process model and on the density of the noise process. This density exploits information about only the previous measurements, without taking into account the latest measurement.

The second step *update* takes place when the new measurement becomes available, and the posterior density is assessed by (5.15), where:

$$p(\mathbf{y}(k)|\mathbf{y}(1) \ldots \mathbf{y}(k-1)) = \int p(\mathbf{y}(k)|\mathbf{x}(k))p(\mathbf{x}(k)|\mathbf{y}(1) \ldots \mathbf{y}(k-1))d\mathbf{x}(k), \tag{5.17}$$

with $p(\mathbf{y}(k)|\mathbf{x}(k))$ related to the process model and to the density of the measurement noise.

Eqs. (5.15) and (5.16) represent the solution for the recursive estimation of the system state vector $\mathbf{x}(k)$. However, these equations cannot be evaluated in the practice, because in general the integrals cannot be determined analytically. Instead, approximated solutions as the Monte Carlo methods can be used, which approximate the Bayesian integrals by finite sums. The resulting filter implementation is called *particle filter*. Several particle filter implementations can be found in literature, as described in [71]. Among these, an ASIR particle filter has been used. The ASIR particle filter is a variant of the Sequential Importance Resampling (SIR) particle filter, where the sampling step is modified to sample, for each particle, an auxiliary variable, corresponding to a particle index, according to a distribution which weights each particle in terms of its compatibility with the current measurements. Then, the new state value is sampled as the offspring of the particle indicated by this auxiliary variable [72]. Thanks to this modification, the ASIR filter is expected to give better results than the SIR particle filter, where the new state variable is sampled without taking into account the current measurements. In particular, the ASIR particle filter operates as it follows.
At each sampling time k, for each particle $i = 1, \ldots, N_s$, the auxiliary variable $\mu^i(k)$ is evaluated. In general, $\mu^i(k)$ is some characterization of $\mathbf{x}(k)$, given $\mathbf{x}^i(k-1)$. In the case of this work, it has been considered the expectation, thus $\mu^i(k) = \mathrm{E}[\mathbf{x}(k)|\mathbf{x}^i(k-1)]$. Then, some first stage weights $\lambda^i(k)$ are evaluated as:

$$\lambda^i(k) = \lambda^i(k-1) \cdot p(\mathbf{y}(k)|\mu^i(k)), \tag{5.18}$$

and normalized by the total number of weights $N_\lambda = \sum_{i=1}^{N_s} \lambda^i(k)$. Such weights are used in a resample phase to evaluate the particle indexes $j(i)$ that are more meaningful, according to the current values of the measurements. A number N_s of particles $\mathbf{x}^i(k)$ are drawn from the conditional probability $p(\mathbf{x}(k)|\mathbf{x}^{j(i)}(k-1))$ This is carried out by generating a process noise sample:

$$\mathbf{v}^i(k) \sim p_n(\mathbf{v}(k-1)) \tag{5.19}$$

where $p_n(\mathbf{v}(k-1))$ is the *pdf* of $\mathbf{v}(k-1)$, and by evaluating

$$\mathbf{x}^i(k) = f_k(\mathbf{x}^{j(i)}(k-1), \mathbf{v}^i(k-1)). \tag{5.20}$$

For each particle, a new weight $w^i(k)$ is evaluated using the following formula:

$$w^i(k) = w^i(k-1) \cdot \frac{p(\mathbf{y}(k))|\mathbf{x}^i(k)}{p(\mathbf{y}(k)|\mu^{j(i)}(k))} \tag{5.21}$$

and again normalized by the total number of weights $N_w = \sum_{i=1}^{N_s} w^i(k)$.

Such weights represent a numerical version of the a posteriori density.

5.5.2 Particle filter for magnetic field estimation and uncertainty evaluation

An ASIR particle filter was designed according to the above process model with the twofold aims of *(i)* estimating the magnetic flux, starting from the voltage measurement of the coil and its longitudinal position, and *(ii)* evaluating the uncertainty of the estimate.

At this aim, the measurement process is to be formulated in the form of (5.13). The description of the function $f_k(\cdot)$ needs to be completed by an a priori knowledge of the magnetic field. Such a knowledge is condensed in a lookup table of the coefficient $\mathcal{C}_{0,0}$, for the values of z in the range $[-0.60,\ 0.60]\,\mathrm{m}$ corresponding to the run of the transducer.

From this, the magnetic flux sensed by each coil is then obtained by summing to the previous value of the flux, the expected increment evaluated according to (5.10), by taking into account the coil tilt ϑ and the radial displacement Δr. In turn, ϑ and Δr are obtained according to a *(nearly) constant position* model where the speeds are modeled with the random Gaussian processes $v_\vartheta(k)$ and $v_{\Delta r}(k)$, with standard deviations 107 µrad and 183 µm, respectively. Noise terms $v_{\Phi,1}$ and $v_{\Phi,2}$, assumed with Gaussian distribution, null mean, and variance equal to 5×10^{-4}, were then added to the flux equations to take into account model uncertainty.

Moreover, the process noise terms $v_z(k)$ and $v_s(k)$, related to the coil motion have been generated using the covariance matrix in (5.9) with a value of σ_a equal to $200\,\mathrm{\mu m/s^2}$.

Therefore, the state vector was defined as:

$$\mathbf{x}(k) = \begin{bmatrix} z(k) & s(k) & \Phi_1(k) & \Phi_2(k) & \vartheta(k) & \Delta r(k) \end{bmatrix}^T . \tag{5.22}$$

The process noise is, instead, represented by the vector:

$$\mathbf{v} = \begin{bmatrix} v_z(k) & v_s(k) & v_\vartheta(k) & v_{\Delta r}(k) & v_{\Phi,1}(k) & v_{\Phi,2}(k) \end{bmatrix} . \tag{5.23}$$

The measurement process is then described by the following state equations:

$$
\begin{aligned}
z(k) &= z(k-1) && + Ts(k-1) + v_z(k-1) \\
s(k) &= s(k-1) && + v_s(k-1) \\
\vartheta(k) &= \vartheta(k-1) && + v_\vartheta(k-1) \\
\Delta r(k) &= \Delta r(k-1) && + v_{\Delta r}(k-1) \\
\Phi_1(k) &= \Phi_1(k-1) && + N_1 \cdot [F(z(k), \vartheta(k), \Delta r(k)) + \\
& && -F(z(k-1), \vartheta(k-1), \Delta r(k-1))] \cdot (1 + v_{\Phi,1}(k-1)) \\
\Phi_2(k) &= \Phi_2(k-1) && + N_2 \cdot [F(z(k)+d, \vartheta(k), \Delta r(k)) + \\
& && -F(z(k-1)+d, \vartheta(k-1), \Delta r(k-1))] \cdot (1 + v_{\Phi,2}(k-1))
\end{aligned}
\tag{5.24}
$$

Output equations are represented by (5.12).

The designed particle filter executes the following steps, at each sampling time k:

1. the auxiliary variable $\mu^i(k)$ is evaluated as the expectation $\mathrm{E}[\mathbf{x}(k)|\mathbf{x}^i(k-1)]$. This is practically achieved by considering null all error terms in (5.24);

2. the first stage weights $\lambda^i(k)$ are evaluated by (5.18) and normalized.

3. a resampling is performed according to the *multinomial resampling* strategy [73] thus obtaining the indexes $j(i)$.

4. N_s trials of the vector $\mathbf{v}$ are generated for each sampling time, according to its pdf;

5. the state equations (5.24) are evaluated to obtain the new values of the particles $\mathbf{x}^i(k)$ using the index $j(i)$ for the previous state;

6. the second stage weights $w^i(k)$ are evaluated by (5.21) and normalized;

5.6 Experimental validation

The uncertainty of the translating coil method was assessed by executing the particle filter described in Section 5.5 on a set of data acquired using the set-up of Fig. 5.1. The processing time was reduced by executing the particle filter with a sampling time of 200 ms.

The particle filter provides, at each sampling time, an estimation of the distribution of all the state variables. For each of them, the mean, the standard deviation, and the 10^{th} and 90^{th} percentiles were evaluated. In particular, the mean value is provided as a posteriori estimate of the state variable. For sake of brevity, only the results on the first coil are reported, because compatible results were obtained on the second coil.

In Fig. 5.13a, the a posteriori estimate of the coil speed is shown. The speed is almost constant around 19.3 mm/s, with an increase in variability for values greater than 0.181 m, where the position measurement resolution changes from 10 µm to 100 µm. In Fig. 5.13b, the standard deviation of the estimated speed is shown. A steep increase after 0.181 m can be noted, where the position accuracy increases.

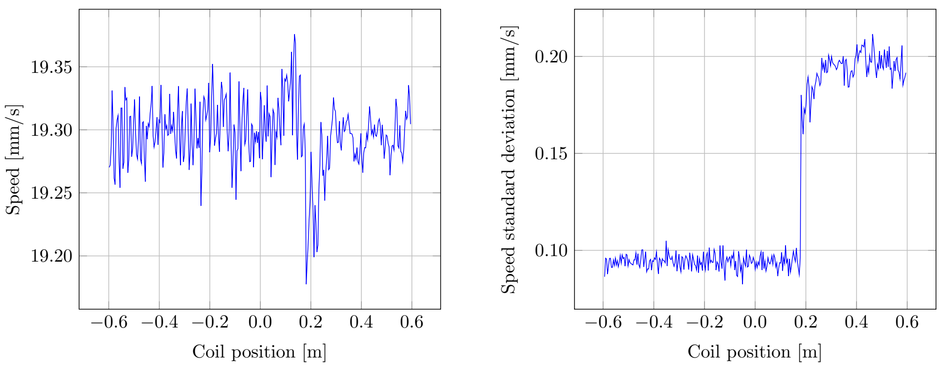

(a) Coil speed estimated by the particle filter. (b) Standard deviation of the estimated speed.

Figure 5.13: Results of speed estimation.

The effect of the position measurement resolution can be also clearly argued from Fig. 5.14, where the standard deviation of the position estimate is shown (in blue), together with the position measurement resolution (in red).

In Fig. 5.15a, the estimated magnetic flux (blue) and the measurements of the Hall probe mapper (red) are compared. As expected, the estimated flux overlies the mapper measures, while making available data even where these are not available. The accuracy of the flux estimation is shown in Fig. 5.15b, where, for each value of the position, the standard deviation of the flux estimation is shown (in red), together with the values corresponding to the 10^{th} (lower blue line) and the 90^{th} (upper blue line) of the distribution of the deviation of the estimated flux from its average. It can be shown that the uncertainty is higher at the center of the magnet, where the flux is higher. The flux uncertainty is mainly determined by the model uncertainty and by the uncertainty of the voltage measurement. An increase of the deviation was then observed for values of the position higher than 0.181 m, due again to the increase in

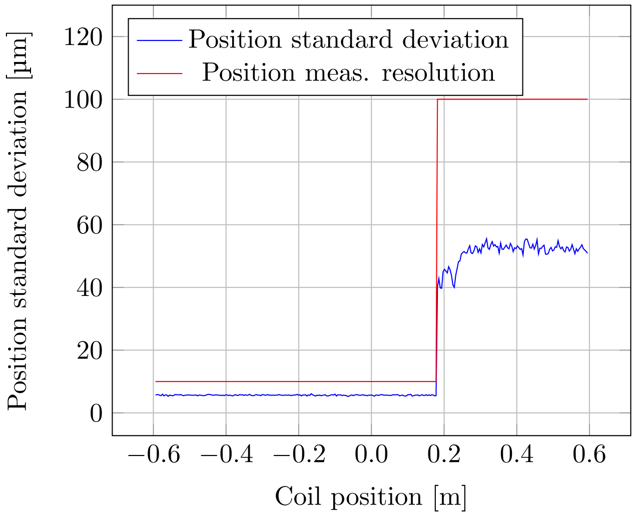

Figure 5.14: Standard deviation of the estimated coils position.

position measurement resolution.

Finally, in Fig. 5.16, the measured (red) voltage and that, estimated (blue) by differentiating the flux estimates, are compared. A good agreement has been observed thus confirming the capability of the ASIR particle filter of following the measurements.

5.7 Discussion

A method for the dynamic measurement and uncertainty analysis of the magnetic flux for axisymmetric magnets by means of the translating-coil method has been presented in this paper. In particular, an analysis of the uncertainty sources, that can contribute to the uncertainty of the field measurements, have been analyzed. The proposed method makes use of a particle filter, able to provide the posterior density of the magnetic flux. The results show that the standard deviation of the estimated flux is lower than 300 µWb, corresponding to about 0.2 %. Further efforts can be concentrated to an improvement of the transport system. Moreover, the acquisition system should be modified in order to reduce the uncertainty of the voltage measurements and the position measurement resolution for positions further than 1 m from the interferometer.

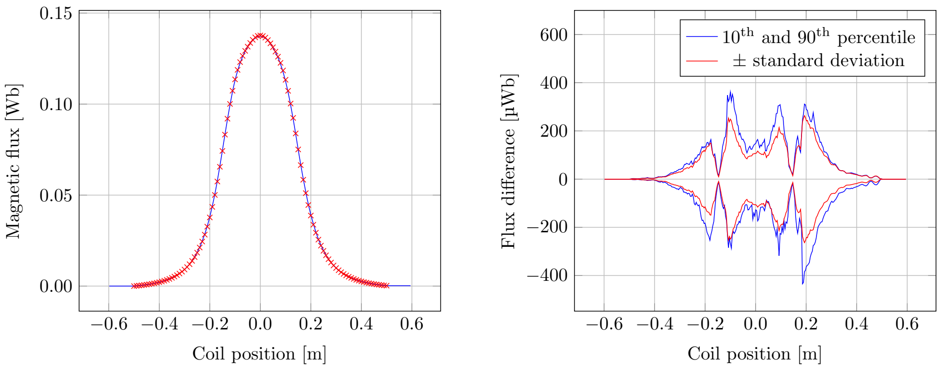

(a) Estimates (blue) and Hall mapper measurements (red) of the flux.

(b) Distribution of field estimate

Figure 5.15: Results of magnetic flux estimation.

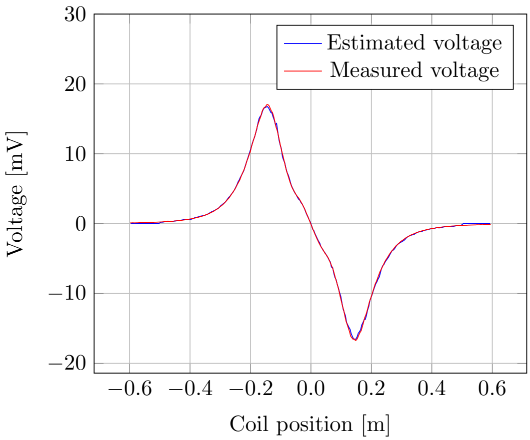

Figure 5.16: Results of the voltage estimation.

Part III

Experimental Results

Chapter 6

Realization of the measuring system

In this chapter, the prototype version of the translating-coils system is presented, where several improvements on the mechanics and electronics of the individual parts have been made, as suggested by the results of the uncertainty analysis of the previous chapter. In particular, a new transport system, the addition of the laser interferometer interface, the inclusion of two Fast Digital Integrators (FDIs), and the integration with the existing CERN Flexible Framework for Magnetic Measurement (FFMM), have led to a new architecture of the measurement system.

6.1 Architecture

The transducer is displaced longitudinally inside the magnet aperture by means of a linear actuator and a voltage is induced at its terminals. A linear laser interferometer measures the transducer position by following a retroreflector that is rigidly connected to its core. Finally, integrating the induced voltage between predefined longitudinal positions allows the flux change to be obtained as a function of the linear position. Fig. 6.1 shows the architecture of the measurement system and the cooperation among the different components. The measurements system is equipped with two Fast Digital

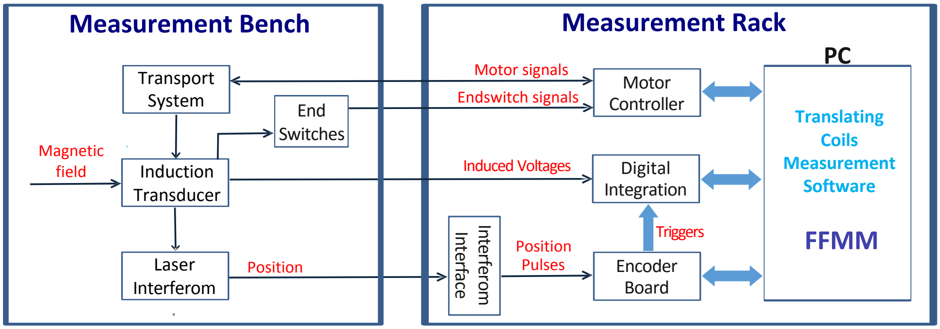

Figure 6.1: Architecture of the translating-coils system

Integrator (FDI) boards [74], an encoder board, and a motor controller, which are remotely driven by a PXI PC running the measurement software, developed in the Flexible Framework for Magnetic Measurements (FFMM) environment [75]. The measurement software, via the motor controller, actuates the transport system and the transducer starts moving. At the same time, the encoder board is initialized and FDIs are put on hold for triggers signals. As the transducer hits the first endswitch on the longitudinal axis (HP in Fig. 5.1), the encoder board starts counting the position pulses coming from the interferometer and generating trigger signals for the FDIs. The induced voltage signals resulting from the series and anti-series combinations of the two coils are acquired and integrated by the FDIs, yielding the flux linkage as a function of the linear position measured with the laser interferometer. This re-parametrization with respect to the linear position eliminates the time-dependence and relaxes the requirements on the homogeneous linear speed of the transport system. The measurement architecture provides an on-the-fly read out of the partial integrals (flux increments), allowing rapid field mapping of the longitudinal and transverse field components with almost arbitrary spatial resolution.

6.2 Implementation of the measuring bench

The construction of the measurement bench had to satisfy some requirements that are intrinsic to magnetic measurements in general, and others that are specific to the translating-coils system. Besides the transducer, this is in particular the case for the transport system and the position measuring system, which operate by moving their components inside the magnetic field. The following requirements need to be satisfied:

- magnetic compatibility - all the system components should be non-magnetic in order to avoid interference with the measured magnetic field; moreover the moving parts should be also non-conductive to avoid eddy currents insurgences.
- mechanical stability - the precision of the measurement strongly depends on the mechanics; any kind of mechanical vibration is a potential source of errors that can generate vibration-induced voltages in the transducer or a loss of precision in the measurement of the position.
- reduced dimension - as highlighted in the following, the transducer and its support should be able to translate through the magnet aperture. Hence, it is really important that the system components have a reduced dimension.

The final version of the translating-coils measurement system is schematically presented in Fig. 6.2. It can be noticed that the mechanical structure of the measurement system is divided in three parts: a table adjustable in height and orientation (pitch and yaw) on which the magnet is placed, an aluminium structure that supports the rail and the linear actuator, and a stable structure to support the laser head and the interferometer. This structure division ensures that the motor vibrations are not transmitted to the magnet under test and, especially, to the laser head and interferometer.

The main uncertainty sources of the measuring system were analyzed in [16] and the transport system was pointed out as the main contribution to the uncertainty budget. For this reason, the bench is equipped with a new transport system with respect to the preliminary version presented in [14]. The new transport system is designed and constructed in-house in order to fit exactly to the technical requirements of the system. It is based on a belt-driven linear actuator driven via a controlled step motor (in gray-violet in Fig. 6.2).

It has to be noticed that the transport system is installed through the solenoid aperture, and what is more important, it should allow the carriage hosting the trans-

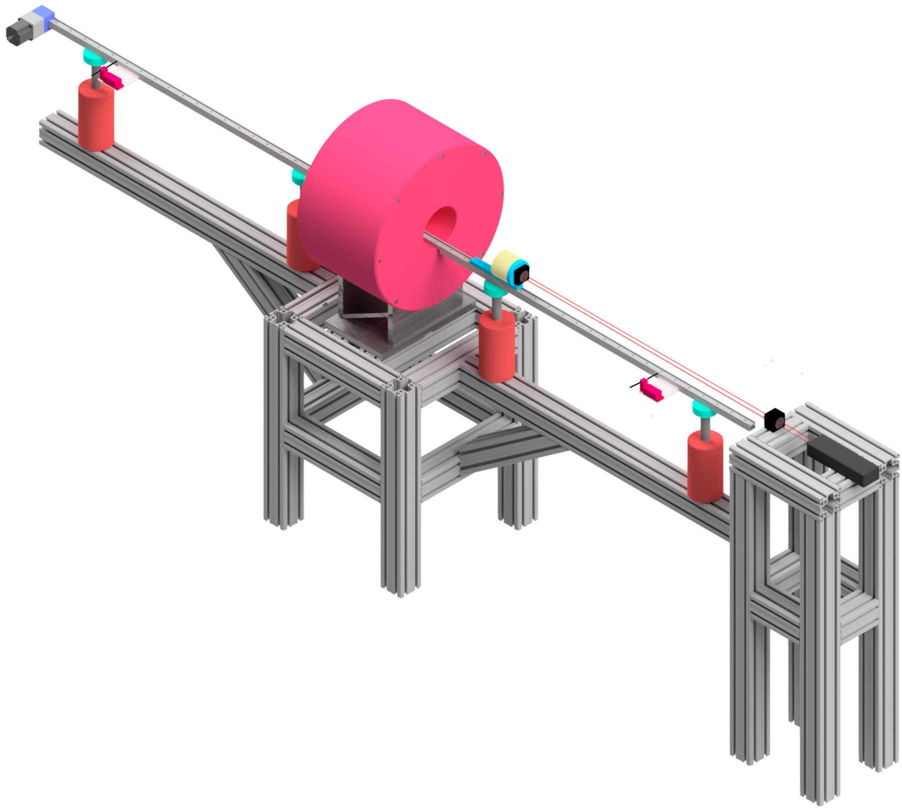

Figure 6.2: Measurement setup consisting of the solenoid magnet (pink), the inductive sensor (yellow), the HPI-3D laser measurement system consisting of the laser head, interferometer and retroreflector (black), the aluminium rail (gray) and the plastic carriage (blue), the stepper motor (gray-violet), two end-switches (purple), and four non-magnetic rail supports (orange).

ducer (in blue in Fig. 6.2) to be centered inside the aperture. This means that the rail and the carriage should have a profile as lower as possible. To achieve this aim it is used a *DryLin N* linear slide from Igus [76]. The chosen version presents an extremely low profile (27 mm rail width, 9.5 mm height) and is available in the required length (3 m) allowing the transducer to move from an initial to a final position, such as to cover the entire fringe field of the solenoid. Through the use of a small spring, the preloaded version of the carriage helps to remove any clearance between the carriage and the rail, minimizing the vibrations during the motion. The initial and final positions are delimited by two endswitches (in purple in Fig. 6.2), that not only send signals to the motor controller but have also the task to start and stop the data acquisition. Independently of the movement direction, at the second endswitch

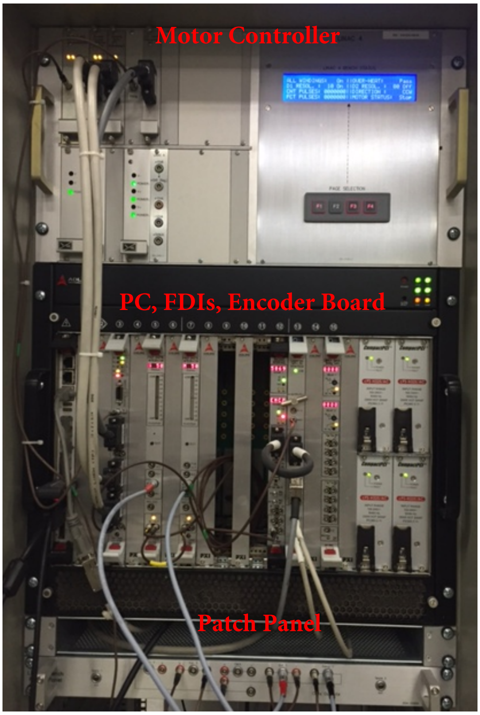

Figure 6.3: Measurement rack.

signal, the motor and the data acquisition are stopped.
The linear laser interferometer, consisting of a laser head, an interferometer and a retro-reflector, is employed for precise recording of the inductive transducer displacement. In particular, the retro-reflector is attached to the transducer and its relative linear motion with respect to the interferometer is detected.
The translation speed and direction are managed by the motor controller (upper side of the measurement rack in Fig. 6.3), which is driven by the measurement software through USB connection. The series and opposite polarity configurations for the sensing coils of the transducer are implemented analogically by a patch panel (lower part of Fig. 6.3), that receives the voltage signals from the coils and sends their combinations to the FDIs. The FDI acquisition is triggered by the encoder board pulses by counting and elaborating a quadrature (A-Quad-B) signal in 5 V CMOS standard coming from the HPI-3D.

Chapter 7

Experimental validation

In this Chapter, the set-up configuration, the measurement results, and the experimental validation of the measurement system are discussed.

The CERN solenoid no. PXMLNABNWC-DA000003, employed as focusing element in the linear accelerator Linac4, was chosen as reference magnet. The solenoid was produced at Danfysik where a campaign of magnetic field measurements was performed to validate the magnet design and production process. These measurements are reported in [77] together with the localization of the magnetic axis and the magnet fiducial information. In particular, the 3D Hall-probe map and the magnet fiducial are used hereinafter to validate the translating-coils measurement system.

7.1 Measurement setup

The Linac4 solenoid and the coordinate system adopted for the magnetic measurements and the experimental validation are shown in Fig.7.1a. The coordinate system is located at the center of the magnet in the z-direction. Fig.7.1b shows the location of the fiducial reference markers used for defining the local coordinate system of the magnet. In Tab.7.1 are summarized the mechanical and electric characteristics of the solenoid chosen for the validation. The longitudinal (B_z) and radial (B_r)

Magnetic length	307 mm
Aperture radius	70 mm
Good field region radius	55 mm
Nominal current	122 A
Electrical resistance at 20 deg.cel	215 mΩ
Inductance	60 mH
Nominal voltage	26, 2 V

Table 7.1: Mechanical and electrical data of the solenoid

components of the magnetic field, obtained with the described measurement setup, are shown respectively in Fig. 7.2 and Fig. 7.3. It has to be noticed that these are integral measurements and represent the field averaged over the coil area (for the longitudinal component) and over the lateral area in between the two coils (for the radial component).

7.2 Results validation

The proposed measurement system is validated by comparison with a single-axis Hall transducer on the reference solenoid. The measurements by the translating coils and the Hall transducer are compared in the good field region of the magnet, namely over a cylindrical volume passing through the solenoid aperture, delimited by the maximum displacement of the mapping system along the longitudinal axis of the solenoid, and by the coils' surface in the transversal plan.

The reference field map was generated by first selecting a position in the xy-plane and then performing the scan along the z-axis. For each xy-point, with a grid from $x = -45$ to $x = +45$ mm and from $y = -45$ to $y = +45$ mm, and a resolution of 5 mm, a full-range scan in the z-axis, from $z = -500$ to $z = 500$ mm, with a resolution of 1 mm, yields 1000 measurement points. As shown in the Fig. 7.4, the Hall measurements are sampled at points throughout the volume of interest, while the translating-coils measurements are "slice-sampled" and represent an integral value over the coil area. Thus, in order to have two sets of measurements data that are compatible and comparable, at each step (1 mm) along the z-axis, the integral of the xy-points that lie inside the coil circumference (red circle in Fig.7.4) is computed. These integral values obtained from the Hall-probe measurements are then compared to the translating-coils measurements at corresponding positions along the z-axis. The position has a direct impact on the measurement results because it can contribute significantly to the error budget of the experimental validation. Therefore, special attention was paid to make sure that the position points are the same for the two measurement systems.

For this purpose, it has to be mentioned that the measurement of the magnet axis and the fiducialization of the solenoid under test have already been performed at CERN and reported in [69]. In particular, the fiducial reference markers (denoted as R1, R2, R3, and R4 in Fig. 7.1b), where the local coordinate system of the magnet is fixed, are given with respect to the magnetic axis (x = 0 mm, y = 0 mm). Therefore, after leveling the magnet to the gravity (it was used as vertical reference, y-axis), the translating-coil transducer was centered and aligned to the magnetic center with a laser tracker system with respect to the reference markers.

The integral values are plotted as a function of the longitudinal position, and Fig. 8.1 shows the longitudinal profiles obtained with the two systems. It can be noticed that there is a good degree of concordance between the measurement results. The absolute differences (B_z Hall $-$ B_z Coil) are plotted in Fig.7.6, where it can be seen that the variations along the full measurement range are contained in an interval smaller than ± 0.3 mT. There are two main contributions in the error budget: the first one is related to the difference of resolution in measuring the longitudinal position between the two systems, 1 mm for the Hall probe and 0.4 mm for the translating-coil system, and the second to the drift of the digital integrator in the translating-coil system.

Although these error contributions can be both minimized with some precautions, the excellent agreement between both measurements confirms the validation of the translating-coils measurement system. In fact, the absolute differences are inside the uncertainty interval of the Hall probe system ($\pm 5 \times 10^{-4}$ T).

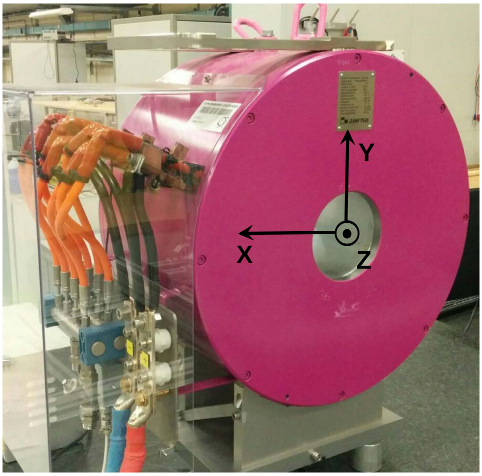

(a)

(b)

Figure 7.1: View of the Linac4 S3 solenoid and coordinate system (a), and location of the fiducial reference markers (denoted as R1, R2, R3, and R4), which define the local coordinate system of the magnet (b).

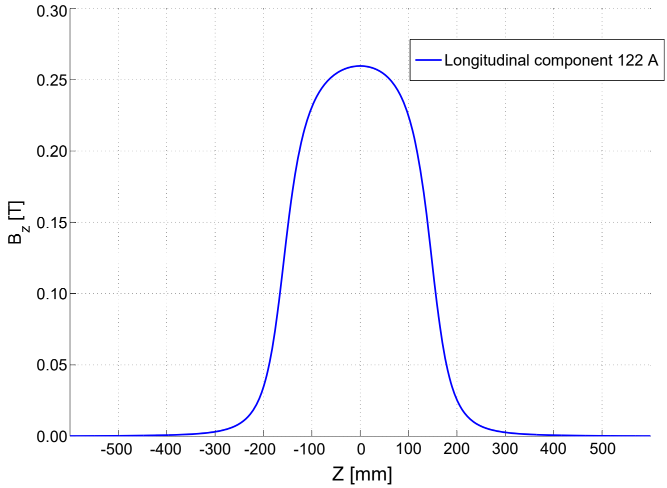

Figure 7.2: Longitudinal component of the magnetic field.

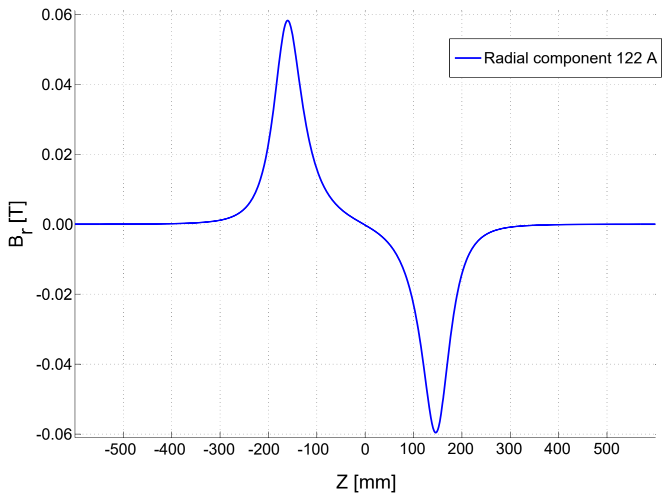

Figure 7.3: Radial component of the magnetic field.

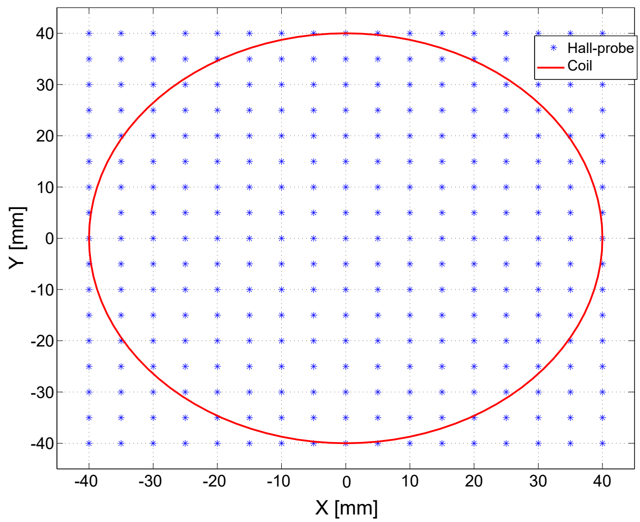

Figure 7.4: Field map and coil area in the transverse xy-plane for a given $z = z*$

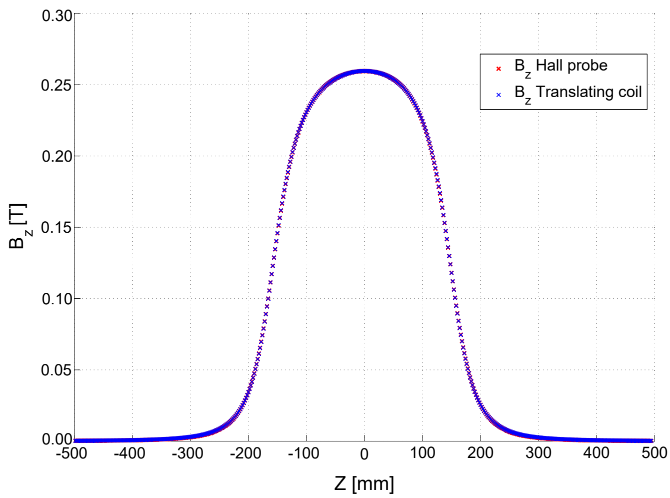

Figure 7.5: Longitudinal profile of the Linac4 solenoid obtained with the two measurement methods.

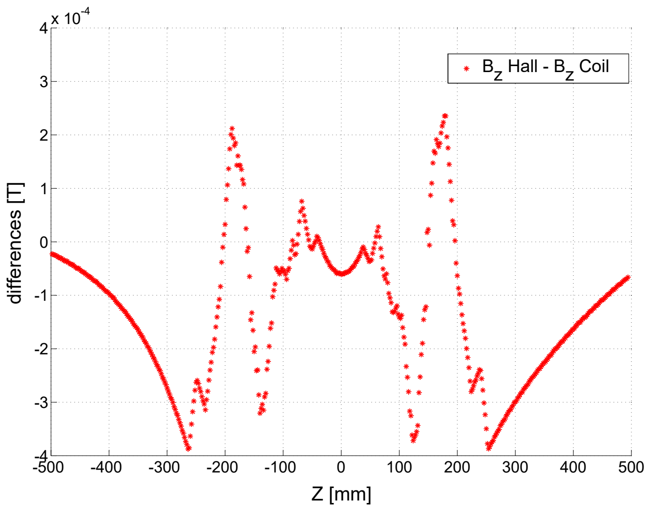

Figure 7.6: Absolute differences between the results of the two measurement methods.

Chapter 8

On-field exploitation

After the successful experimental validation, this Chapter presents on-field measurements by means of the translating-coils system. In particular, the results of the measurement campaign on the Linac3 solenoid magnet ITL.SOL01 [78] and a shielding system based on μ-metal material are reported.

8.1 Measurements of a Linac3 solenoid

Linear accelerator 3 (Linac3) is the starting point in the heavy ion injector chain of the Large Hadron Collider (LHC), providing charged heavy ion beams for the CERN experimental program. The ion beams are produced with a 14.5 GHz Electron Cyclotron Resonance (ECR) ion source and are selected with a spectrometer. Immediately after the ion source, a focusing solenoid (ITL.SOL01) is in charge of bringing a beam as small as possible to the spectrometer and avoid any loss of intensity [23].
The upgrade program of the Linac3 in preparation for the future high luminosity LHC aims to reduce the beam losses taking place immediately downstream from the ion source and improve the transport of the beam in the following Low Energy Beam Transport (LEBT) section [79]. Magnetic measurements of the solenoid magnet ITL.SOL01 are a part of the upgrade program.
Considering the short time scheduled for the magnetic measurements and the main interest in characterizing the integral field as a function of the longitudinal position, it was decided to perform the measurements by means of the translating-coils system. Tab.8.1 shows mechanical and electric characteristics of the solenoid to be measured. The inductive transducer (diameter of 85 mm) was centered on the solenoid axis

Magnet dimensions (length, width, height)	$320 \times 392 \times 392$ mm
Solenoid bore diameter	110 mm
Max axial field	$0,625$ T
Magnet resistance (all coils)	435 mΩ
Nominal current	133 A
Maximum allowable current	220 A
Maximum voltage	103 V

Table 8.1: Mechanical and electrical data of the Linac3 ITL.SOL01

(Fig.7.6), fully covering the central region of the solenoid aperture (diameter of 110 mm) that affects the dynamics of the ion beams. The limited voltage of the power converter (Transtechnic ± 600 A ± 40 V) did not allow to power the magnet at its nominal current. For this reason a series of measurements were performed, starting from a current value of $I_{nom}/8$ (16.625 A) and going up at its multiples until the maximum possible (83.125 A). The measured integrals of the longitudinal and radial components as a function of the longitudinal position are shown in in Fig.8.2 and in Fig.8.3 respectively. Fig.8.4 illustrates the maximum values of the longitudinal and radial fields as function of the supply current. The fitting line could be used to extract the field values at the nominal or higher currents.

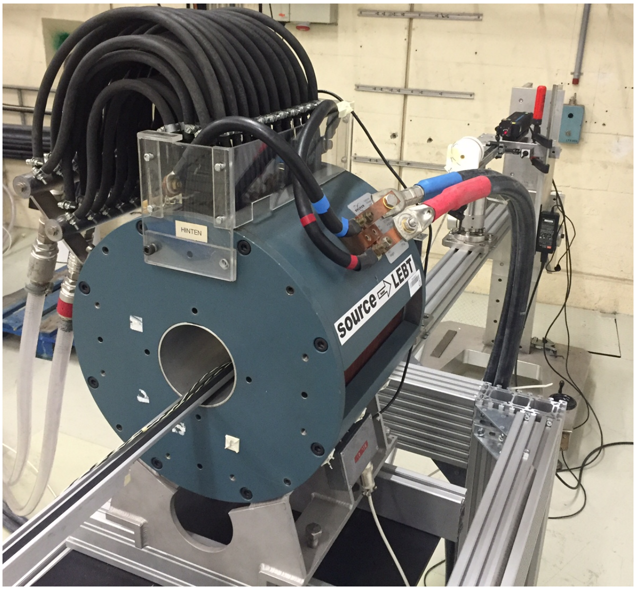

Figure 8.1: Linac3 ITL.SOL01 on the translating-coils bench.

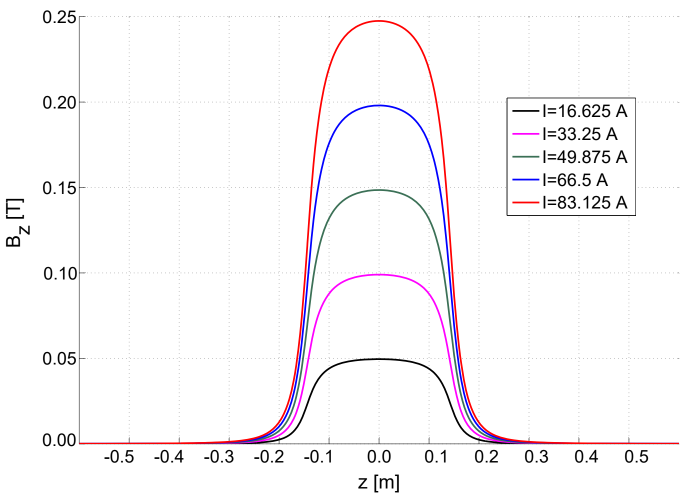

Figure 8.2: Longitudinal profile of the Linac3 solenoid for different supply currents.

8.2 Measurements of μ-metal tubes

A measurement campaign is currently undergoing at CERN for testing μ-metal material used for magnetic shielding in the cavities of the Superconducting Proton Linac.

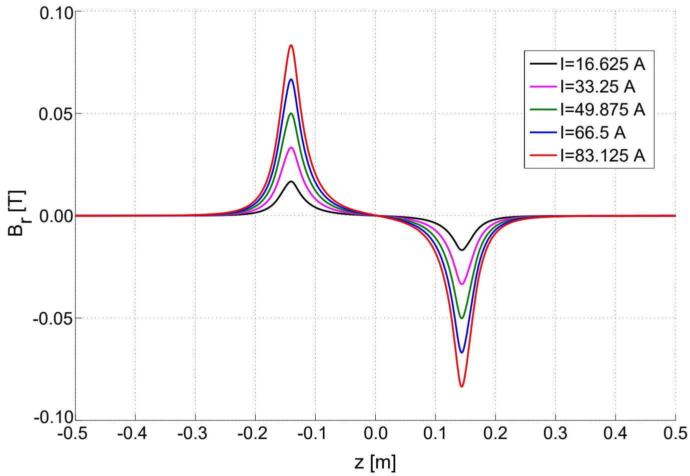

Figure 8.3: Radial profile of the Linac3 solenoid for different supply currents.

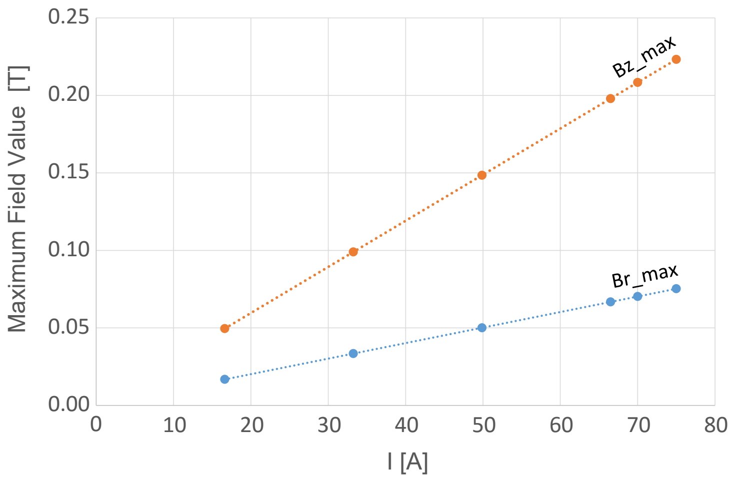

Figure 8.4: Maximum field values of B_z and B_r as a function of the supply current I.

The shield is designed to reduce the background field on the cavity and, for this purpose, tubes of different lengths made with a 1-mm-thick μ-metal sheet have been fabricated. In order to understand the typical shielding efficiency for such a material, it was decided to test the μ-metal tubes inside the aperture of a solenoid magnet for

different field levels. Measuring the magnetic field outside and inside the tubes is very useful during the design process for validating simulations and calculations.
The translating-coils system turned out to be very suitable for these kind of magnetic field measurements. In fact, highly permeable tubes of different lengths were easily tested in the measurement setup showed in in Fig.8.5. A series of measurements were

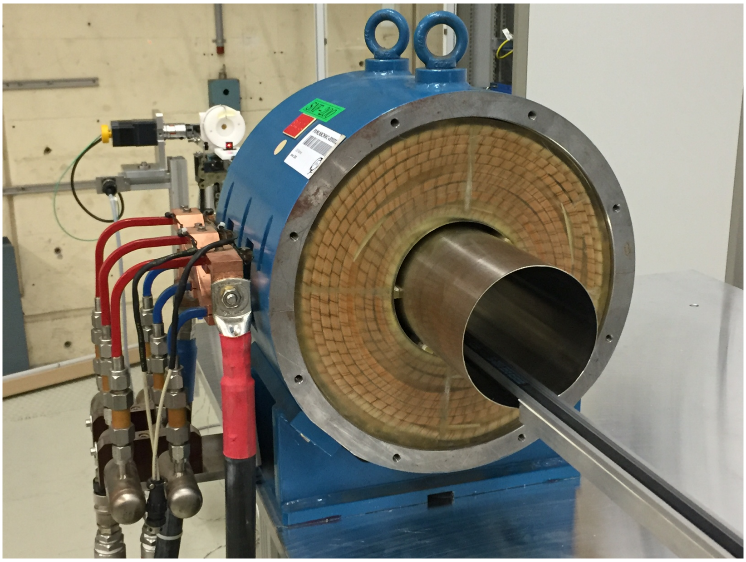

Figure 8.5: Measurement setup for the test of the shielding tubes.

performed for different field levels by increasing the current in the magnet in a range from 0 to 1 A. Initially the measurements were carried out without the μ-metal tube, and then repeated with the tube under test installed, in order to directly evaluate the effect of the shielding by comparison. In Fig.8.6 and Fig.8.7 are respectively illustrated the measurements of the longitudinal and radial components for a current of 1 A. It can be noticed that the 300 mm tube performs a better shielding at the tube center whereas the 600 mm one shields more at its ends. These measurements concern the testing phase before the heat treatment of the shielding tubes. A similar measurement campaign is foreseen after a heat treatment in order to see the effect of the welding and annealing.

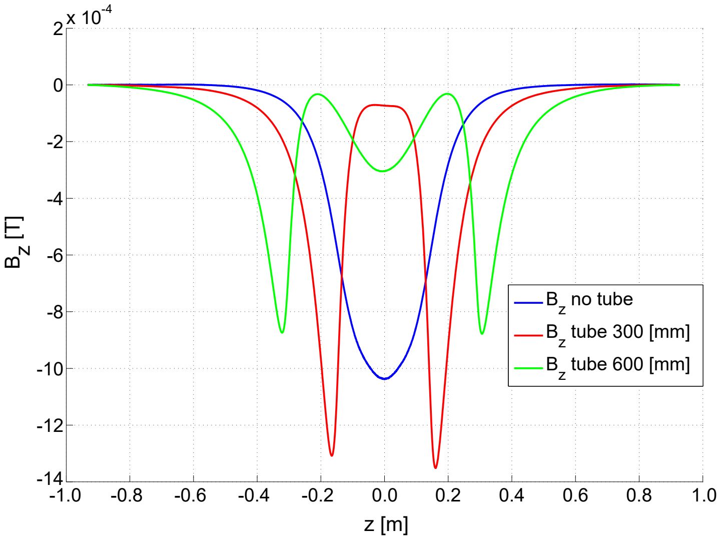

Figure 8.6: Longitudinal components measured by the translating-coils system: with (300 mm and 600 mm) and without the shielding tubes. The solenoid is powered with a current of 1 A.

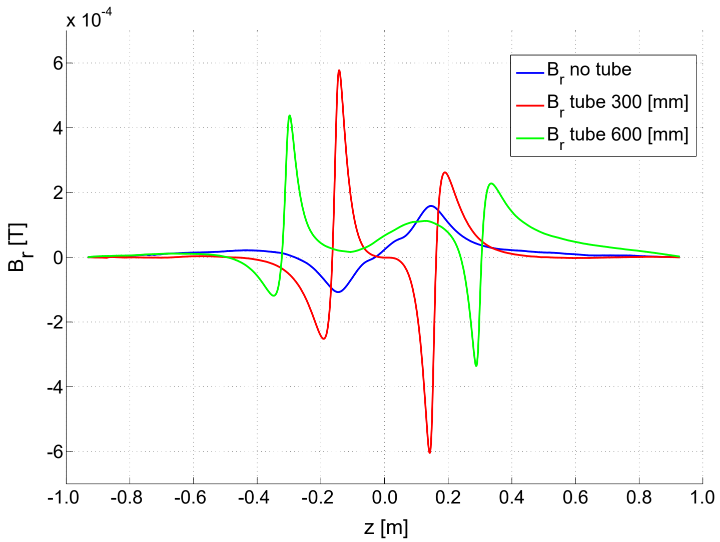

Figure 8.7: Radial components measured by the translating-coils system: with (300 mm and 600 mm) and without the shielding tubes. The solenoid is powered with a current of 1 A.

Conclusions

In this Thesis, a reliable and high-speed measurement system based on translating coils for characterizing axially-symmetric magnets has been designed, constructed and validated. The system yields a measurement of the longitudinal and transverse components of the magnetic field as a function of the longitudinal position. The field integrals F_1 and F_2 are obtained more precisely and in a fraction of the time needed by traditional techniques.

The state-of-the-art presented in **Chapter 1** and **Chapter 2** has highlighted the lack in the present literature of a method specifically designed for measuring axisymmetric magnets. In fact, these magnets are routinely tested with general-purpose systems that are poorly adapted to exploit their field symmetry and geometrical characteristics.

In this context, given the importance of the integrated field or the gradient field of axisymmetric magnets for beam dynamics studies, a new measurement method based on moving search coils has been proposed in **Chapter 3**. The translating-coils method is designed in order to allow a direct measurement of the focusing parameters in cylindrically-symmetric magnets. By designing a custom transducer, the method allows to measure the gradient and integrated fields in a single set of measurements (obtainable in few minutes), thereby greatly improving both measurement speed and precision.

The experimental proof-of-principle demonstration of the method is performed in comparison with a Hall-probe mapping system and the results have been presented in **Chapter 4**. The effective surface of the coils is calibrated by flipping them upside down in an NMR-mapped reference dipole magnet. For the longitudinal distance between the coils, an in-situ magnetic calibration was chosen. The radial and longitudinal components of a CERN solenoid measured by the proposed method were compared to the Hall-probe results with satisfying agreement. Furthermore, from the measurement data, the field integrals F_1 and F_2 were evaluated.

A method for the dynamic measurement and uncertainty analysis of the magnetic flux for axisymmetric magnets by means of the translating-coil method has been presented in **Chapter 5**. In particular, an analysis of the uncertainty sources, that can contribute to the uncertainty of the field measurements, have been analyzed. The proposed method makes use of an ASIR particle filter, able to provide the posterior density of the magnetic flux. The results show that the standard deviation of the estimated flux is lower than 300 µWb, corresponding to about 0.2 %. Further efforts can be concentrated to an improvement of the transport system. Moreover, the acquisition system should be modified in order to reduce the uncertainty of the voltage measurements and the position measurement resolution for relative distances farther than 1 m from the interferometer.

As suggested by the uncertainty analysis results, a big effort was made to improve the mechanics and electronics of the individual components in the final version of the translating-coils system. These improvements and the new architecture of the system have been described in **Chapter 6**. In particular, the measurements system is equipped with two Fast Digital Integrator (FDI) boards, an encoder board including an interferometer interface, and a motor controller, which are remotely driven by a PXI PC running the measurement software. All the system instrumentation and the software were integrated in the FFMM CERN standard, leading to a fully automatized measuring system.

The improved system was validated experimentally as showed in **Chapter 7**. The set-up configuration, the measurement results, and the experimental validation of the measurement system were discussed. As reference magnet was chosen the CERN solenoid no. PXMLNABNWC-DA000003, employed as focusing element in the linear accelerator Linac4. The radial and longitudinal components of the magnet under test have been measured and the results checked against the corresponding references. The absolute differences $[B_z(\text{Reference}) - B_z(\text{Measured})]$ along the full measurement range are contained in an interval smaller than ± 0.3 mT, demonstrating an excellent agreement of the results.

Finally, **Chapter 8** illustrates two examples of axially-symmetric systems where the translating-coils system resulted a more appropriate solution with respect to other testing methods. This was particularly the case for a Linac3 solenoid at CERN, which had to be taken out of the machine and tested during a run stop, and, therefore, a really short time was scheduled for the magnetic measurements. The magnet was successfully tested by the translating-coils system and sent back in time for the machine restart. The on-field exploitation showed the advantages of the translating-coils system with respect to other testing instruments, confirmed the efficiency and the accuracy of the measurement system.

Future scientific challenges include:

- determination of the the magnetic axis from the measurement data;
- theoretical studies for the reconstruction of 3D magnetic fields from the measurement data to further advance the assessment of the local field.

Possible technical developments regard:

- the construction of inductive transducers based on Helmholtz-like system coils for a direct measurement of higher order harmonics;
- a transducer based on concentric PCB-coils of different radii for a field mapping in the transversal plane.

References

[1] L Bottura and KN Henrichsen. Field measurements. Technical report, CERN, 2002.

[2] Alex Chao. *Handbook of accelerator physics and engineering*. World scientific, 1999.

[3] David B Williams and C Barry Carter. *The transmission electron microscope*. Springer, 1996.

[4] Joseph Bisognano, D Eisert, MV Fisher, MA Green, K Jacobs, KJ Kleman, J Kulpin, GC Rogers, JE Lawler, and D Yavuz. Progress toward the wisconsin free electron laser. Technical report, Thomas Jefferson National Accelerator Facility, Newport News, VA (United States), 2011.

[5] I. Hofmann. Performance of solenoids versus quadrupoles in focusing and energy selection of laser accelerated protons. *Physical Review Special Topics-Accelerators and Beams*, 16(4), 2013.

[6] Ingo Hofmann, Jürgen Meyer-ter Vehn, Xueqing Yan, Anna Orzhekhovskaya, and Stepan Yaramyshev. Collection and focusing of laser accelerated ion beams for therapy applications. *Physical Review Special Topics-Accelerators and Beams*, 14(3):031304, 2011.

[7] AN Mirzoian, PN Ostroumov, GV Romanov, and AP Fateev. Increase of injection efficiency in a high current linear proton accelerator. *Journal of Technical Physics*, 25:710–713, 1980.

[8] B Berkes. *Hall generators, CAS, Magnetic Measurement and Alignment, Hyatt Conference Centre, Montreux, Switzerland, 16-20 March 1992: Proceedings*, volume 92. Cern, 1992.

[9] K. H. Park, Y. K. Jung, D. E. Kim, H. G. Lee, S. J. Park, C. W. Chung, and B. K. Kang. Field mapping system for solenoid magnet. In *AIP Conf. Proc.*, volume 879, pages 260–263, June 2007.

[10] Dino Zangrando and Richard P Walker. A stretched wire system for accurate integrated magnetic field measurements in insertion devices. *Nuclear Instruments and Methods in Physics Research Section A: Accelerators, Spectrometers, Detectors and Associated Equipment*, 376(2):275–282, 1996.

[11] P. Arpaia, M. Buzio, C. Petrone, S. Russenschuck, and L. Walckiers. Multipole correction of stretched-wire measurements of field-gradients in quadrupole accelerator magnets. *Journal of Instrumentation*, 8(08), 2013.

[12] P Arpaia, C Petrone, S Russenschuck, and L Walckiers. Vibrating-wire measurement method for centering and alignment of solenoids. *Journal of Instrumentation*, 8(11):P11006, 2013.

[13] P Arpaia, M Buzio, M Kazazi, and S Russenschuck. A fluxmeter based on translating coils for axially-symmetric magnets. *Proceedings of the 20th IMEKO TC4*, 2014.

[14] P Arpaia, M Buzio, M Kazazi, and S Russenschuck. Proof-of-principle demonstration of a translating coils-based method for measuring the magnetic field of axially-symmetric magnets. *Journal of Instrumentation*, 10(02):P02004, 2015.

[15] P. Arpaia, M. Buzio, L. De Vito, M. Kazazi, and S. Russenschuck. Uncertainty analysis for a moving fluxmeter. In *Proc. of the XXI World Congress*, pages 890–894, Aug. 2015.

[16] P Arpaia, L De Vito, and M Kazazi. Dynamic measurement and uncertainty analysis of axially-symmetric magnetic fields by means of a particle filter. *Metrologia*, 2016.

[17] P Arpaia, M Buzio, M Kazazi, and S Russenschuck. Measurement system based on translating coils for testing axially-symmetric magnets. *Journal of Instrumentation*, 2016.

[18] PR Sarma. Focusing properties and transfer matrix of elliptic solenoid magnets. *The European Physical Journal Plus*, 126(5):1–8, 2011.

[19] Martin Reiser. *Theory and design of charged particle beams.* John Wiley & Sons, 2008.

[20] Nilangshu K Das, Parthasarathi Barat, Sounak Dey, and Tammana Jayakumar. Design of miniature coil to generate uniform magnetic field. *Progress In Electromagnetics Research M*, 34:99–105, 2014.

[21] David E Bordelon, Robert C Goldstein, Valentin S Nemkov, Ananda Kumar, John K Jackowski, Theodore L DeWeese, and Robert Ivkov. Modified solenoid coil that efficiently produces high amplitude ac magnetic fields with enhanced uniformity for biomedical applications. *Magnetics, IEEE Transactions on*, 48(1):47–52, 2012.

[22] LM Hein, G Bellodi, JB Lallement, AM Lombardi, O Midttun, P Posocco, R Scrivens, et al. Linac4 low energy beam measurements. In *Conf. Proc.*, volume 1205201, page THPPP048, 2012.

[23] V Coco, J Chamings, AM Lombardi, E Sargsyan, R Scrivens, et al. Acceleration of several charge states of lead ion in cern linac3. In *Proc. Linac*, 2004.

[24] G Davis, VV Kashikhin, T Page, I Terechkine, J Tompkins, and T Wokas. Designing focusing solenoids for superconducting rf accelerators. *Applied Superconductivity, IEEE Transactions on*, 17(2):1221–1224, 2007.

[25] I Terechkine, J Di-Marco, J Tompkins, T Page, Y Huang, G Appollinari, D Orris, R Rabehl, and M Tartaglia. Focusing solenoids for the hins linac front end. In *Conf. Proc.*, volume 809292, pages 82–84, 2008.

[26] R Webber, G Apollinari, et al. Overview and status update of the fermilab hins linac r&d program. In *this conference*, 2009.

[27] I Terechkine, W Schappert, J DiMarco, M Tartaglia, et al. Solenoid-based focusing in a proton linac. Technical report, 2010.

[28] G. Nielsen, N. Hauge, E. Krauthammer, K. Thaarup, L. O. Baandrup, and A. Baurichter. Superconducting solenoids for rf accelerators and electron guns. *IEEE Transactions on Applied Superconductivity*, 24(3):1–5, June 2014.

[29] R Legg, JJ Bisognano, M Bissen, R Bosch, D Eisert, M Fisher, M Green, K Kleman, J Kulpin, J Lawler, et al. Status of the wisconsin srf gun. In *Proceeding of this Conference, New Orleans, LA*, 2012.

[30] Y Kadi, D Parchet, R Catherall, W Venturini Delsolaro, E Siesling, MA Fraser, Y Blumenfeld, S Calatroni, B Goddard, AP Bernardes, et al. Status and future

perspectives of the hie-isolde project at cern. In *Conf. Proc.*, volume 1205201, page MOOBA02, 2012.

[31] RE Laxdal, RJ Dawson, M Marchetto, AK Mitra, WR Rawnsley, T Ries, I Sekachev, V Zvyagintsev, et al. Isac-ii superconducting linac upgrade–design and status. In *this conference*, 2008.

[32] Stephen D Holmes. Project x: A multi-mw proton source at fermilab. *IPAC10, Kyoto, Japan, May*, 2010.

[33] M Leitner, J Bierwagen, J Binkowski, S Bricker, C Compton, J Crisp, L Dubbs, K Elliot, A Facco, A Fila, et al. Design status of the srf linac systems for the facility for rare isotope beams. *Proc of SRF2011, Chicago*, 2011.

[34] S Sanfilippo. Hall probes: physics and application to magnetometry. *arXiv preprint arXiv:1103.1271*, 2011.

[35] M Buehler, A Bross, Christopher Hess, D Orris, R Pilipenko, R Preece, C Sylvester, M Tartaglia, J Tompkins, and S Virostek. Magnetic measurements for a mice spectrometer solenoid. *Applied Superconductivity, IEEE Transactions on*, 23(3):4500104–4500104, 2013.

[36] KH Park, YG Jung, DE Kim, HG Lee, SJ Park, CH Chung, and BK Kang. A new method of field measurement for solenoid magnet. *Journal of Korean Physical Society*, 50:950, 2007.

[37] D Alesini, S Bertolucci, ME Biagini, C Biscari, R Boni, M Boscolo, M Castellano, A Clozza, G Di Pirro, A Drago, et al. Status of the sparc project. *Nuclear Instruments and Methods in Physics Research Section A: Accelerators, Spectrometers, Detectors and Associated Equipment*, 528(1):586–590, 2004.

[38] B Bolli, S Ceravolo, M Esposito, P Iorio, F Iungo M Paris, C Sanelli, F Sardone, F Sgamma, M Troiani, G Bazzano, et al. Mechanical and magnetic qualification of the focusing solenoids for sparc. Technical report, SPARC-ME-07/001, 2 March, 2007.

[39] R Ostojic, Ron Coleman, I Fang, Michael Lamm, Jason Miller, T Page, Zhen Tang, M Tartaglia, and R Wands. Challenges in the design of the detector solenoid for the mu2e experiment. *Applied Superconductivity, IEEE Transactions on*, 23(3):4500404–4500404, 2013.

[40] M Buehler, S Gluchko, ML Lopes, C Orozco, M Tartaglia, and J Tompkins. Mu2e magnetic measurement studies. *Applied Superconductivity, IEEE Transactions on*, 24(3):1–4, 2014.

[41] V Bocharov, A Bubley, S Konstantinov, V Panasyuk, and V Parkhomchuk. Precise measurements of a magnetic field at the solenoids for low energy coolers. In *AIP Conference Proceedings*, volume 821, page 360, 2006.

[42] VN Bocharov, AV Bublei, SG Konstantinov, VM Panasyuk, and VV Parkhomchuk. Precision measurements and compensation for the transverse components of the solenoids' magnetic field. *Instruments and Experimental Techniques*, 48(6):772–779, 2005.

[43] S Nagaitsev, A Shemyakin, S Seletsky, and V Tupikov. Field measurements in the cooling section solenoid for the recycler cooler. In *Proceedings of EPAC*, Paris, 2002.

[44] C Crawford, E McCrory, S Nagaitsev, A Shemyakin, V Bocharov, A Bubley, V Parkhomchuk, V Tupikov, and S Seletsky. Fermilab electron cooling project: field measurements in the cooling section solenoid. In *Particle Accelerator Conference, 2001. PAC 2001. Proceedings of the 2001*, volume 1, pages 195–197. IEEE, 2001.

[45] V Tupikov, Grigory M Kazakevich, Lionel R Prost, M Sutherland, A Shemyakin, Thomas K Kroc, S Nagaitsev, CW Schmidt, and A Warner. Magnetic field measurement and compensation in the recycler electron cooler. In *AIP Conf. Proc.*, volume 821, pages 375–379, 2005.

[46] Animesh Jain. Plans for measurement of field straightness in the solenoids for the electron lens system for rhic. 17th International Magnetic Measurement Workshop (IMMW17), September 2011.

[47] M. Anerella, W. Fischer, R. Gupta, A. Jain, P. Joshi, P. Kovach, A. Marone, A. Pikin, S. Plate, J. Tuozzolo, and P. Wanderer. Mechanical design and construction of superconducting e-lens solenoid magnet system for rhic head-on beam-beam compensation. *Applied Superconductivity, IEEE Transactions on*, 24(3):1–4, June 2014.

[48] I Frollo, P Andrisand, and I Strolka. Measuring method and magnetic field homogeneity optimisation for magnets used in nmr-imaging. *Measurement science review*, 1(1):9–12, 2001.

[49] Ken-ichi Sasaki, Michinaka Sugano, Hiromi Iinuma, Toru Ogitsu, Naohito Saito, Koichiro Shimomura, and Akira Yamamoto. Development status of superconducting solenoid for the muhfs experiment at the j-parc. In *Journal of Physics: Conference Series*, volume 408, page 012074. IOP Publishing, 2013.

[50] Ahovi Kponou, Alexander Pikin, Edward Beebe, and James Alessi. Analysis of the magnetic field measured by a rotating hall probe in a solenoid to locate its magnetic axis. In *Electron beam ion sources and traps and their applications: 8th International Symposium*, volume 572, pages 178–187. AIP Publishing, 2001.

[51] KH Park, YK Jung, DE Kim, HG Lee, SJ Park, CW Chung, and BK Kang. Field mapping system for solenoid magnet. In *Synchroton radiation intrumentation: Ninth International Conference on Synchrotron Radiation Instrumentation*, volume 879, pages 260–263. AIP Publishing, 2007.

[52] J DiMarco, Y Huang, DF Orris, TM Page, R Rabehl, MA Tartaglia, I Terechkine, and JC Tompkins. Solenoid magnet alignment at fermilab. *IMMW-16, Switzerland, October*, 2009.

[53] E Joseph DiMarco, Ali M Hemmati, Darryl F Orris, Thomas M Page, Roger H Rabehl, Michael A Tartaglia, Iouri Terechkine, and John C Tompkins. Certification of superconducting solenoid-based focusing lenses. *Applied Superconductivity, IEEE Transactions on*, 21(3):1817–1820, 2011.

[54] E Joseph DiMarco, Emil Khabiboulline, Darryl F Orris, Michael A Tartaglia, and Iouri Terechkine. Superconducting solenoid lens for a high energy part of a proton linac front end. *Applied Superconductivity, IEEE Transactions on*, 23(3):4100905–4100905, 2013.

[55] P Arpaia, C Petrone, S Russenschuck, and L Walckiers. Vibrating-wire measurement method for centering and alignment of solenoids. *Journal of Instrumentation*, 8(11):P11006, 2013.

[56] P Arpaia, M Buzio, J Garcia Perez, C Petrone, S Russenschuck, and L Walckiers. Measuring field multipoles in accelerator magnets with small-apertures by an oscillating wire moved on a circular trajectory. *Journal of Instrumentation*, 7(05):P05003, 2012.

[57] P Arpaia, L Bottura, L Fiscarelli, and L Walckiers. Performance of a fast digital integrator in on-field magnetic measurements for particle accelerators. *Review of Scientific Instruments*, 83(2):024702, 2012.

[58] M Buzio. Fabrication and calibration of search coils. *arXiv preprint arXiv:1104.0803*, 2011.

[59] L Walckiers. Magnetic measurement with coils and wires. *arXiv preprint arXiv:1104.3784*, 2011.

[60] National instruments website: http://www.ni.com.

[61] Lasertex website: http://www.lasertex.eu.

[62] P Arpaia, M Buzio, G Golluccio, and L Walckiers. In situ calibration of rotating sensor coils for magnet testing. *Review of Scientific Instruments*, 83(1):013306, 2012.

[63] E Garcia, T Hausotte, and A Amthor. Bayes filter for dynamic coordinate measurements–accuracy improvment, data fusion and measurement uncertainty evaluation. *Measurement*, 46(9):3737–3744, 2013.

[64] BIPM, IEC, IFCC, ISO, IUPAC, IUPAP, and OIML. Evaluation of measurement data - guide to the expression of uncertainty in measurement, 2008.

[65] BIPM, IEC, IFCC, ISO, IUPAC, IUPAP, and OIML. Evaluation of measurement data - supplement 1 to the "guide to the expression of uncertainty in measurement" - propagation of distributions using a monte carlo method, 2008.

[66] C. Elster and A. Link. Uncertainty evaluation for dynamic measurements modelled by a linear time-invariant system. *Metrologia*, 45(4):464–473, 2008.

[67] S Eichstädt, C Elster, J Esward, T, and P Hessling, J. Deconvolution filters for the analysis of dynamic measurement processes: a tutorial. *Metrologia*, 47(5):522–533, 2010.

[68] S. Eichstädt, A. Link, P. Harris, and C. Elster. Efficient implementation of a Monte Carlo method for uncertainty evaluation in dynamic measurements. *Metrologia*, 49(3):401–410, 2012.

[69] A Beaumont, O Crettiez, and G Deferne. Magnetic axis and fiducialization of linac4 solenoid pxmlnabnwc-da000003. *CERN Report*, 2013.

[70] X. Rong Li and V.P. Jilkov. Survey of maneuvering target tracking. part I: dynamic models. *IEEE Transactions on Aerospace and Electronic Systems*, 39(4):1333–1364, 2003.

[71] M Sanjeev Arulampalam, Simon Maskell, Neil Gordon, and Tim Clapp. A tutorial on particle filters for online nonlinear/non-gaussian bayesian tracking. *Signal Processing, IEEE Transactions on*, 50(2):174–188, 2002.

[72] Nick Whiteley and Adam M. Johansen. Auxiliary particle filtering: recent developments. In David Barber, A. Taylan Cemgil, and Silvia Chiappa, editors, *Bayesian time series models*, chapter 3. Cambridge University Press, 2011.

[73] B. G. Sileshi, C. Ferrer, and J. Oliver. Particle filters and resampling techniques: Importance in computational complexity analysis. In *2013 Conference on Design and Architectures for Signal and Image Processing (DASIP)*, pages 319–325, Oct. 2013.

[74] P Arpaia, L Bottura, L Fiscarelli, and L Walckiers. Performance of a fast digital integrator in on-field magnetic measurements for particle accelerators. *Review of Scientific Instruments*, 83(2):024702, 2012.

[75] Pasquale Arpaia, Marco Buzio, Lucio Fiscarelli, and Vitaliano Inglese. A software framework for developing measurement applications under variable requirements. *Review of Scientific Instruments*, 83(11):115103, 2012.

[76] Igus website: http://www.igus.com/.

[77] Danfysik. "quality assurance report and assembly drawing for 1 pcs. of solenoid magnet". CERN no. PXMLNABNWC Serial no. DA 000003.

[78] J Chamings. Beam profile measurements to calculate emittance in the lebt of linac 3. Technical report, RS Note 2003-21.

[79] V Toivanen, G Bellodi, V Dimov, D Küchler, AM Lombardi, and M Maintrot. Upgrade of the beam extraction system of the gts-lhc electron cyclotron resonance ion source at cern. *Review of Scientific Instruments*, 87(2):02B912, 2016.

List of Figures

List of Tables